

CONFIDENTIAL

MARTIN MARIETTA ENERGY SYSTEMS LIBRARIES

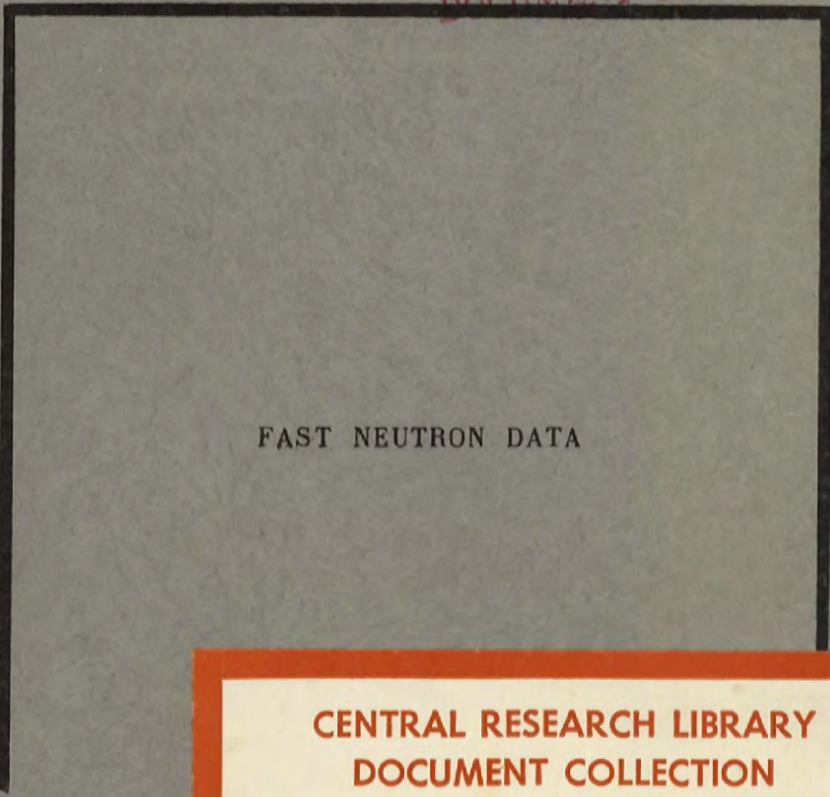


3 4456 0360442 8

ORNL-433
PHYSICS-GENERAL

2A

CENTRAL RESEARCH LIBRARY
DOCUMENT COLLECTION



FAST NEUTRON DATA



**CENTRAL RESEARCH LIBRARY
DOCUMENT COLLECTION**

LIBRARY LOAN COPY

DO NOT TRANSFER TO ANOTHER PERSON

If you wish someone else to see this document,
send in name with document and the library will
arrange a loan.

OAK RIDGE NATIONAL LABORATORY
OPERATED BY
CARBIDE AND CARBON CHEMICALS DIVISION
UNION CARBIDE AND CARBON CORPORATION

UCC
POST OFFICE BOX P
OAK RIDGE, TENNESSEE

CONFIDENTIAL



ORNL 433

This document consists of
96 pages.
Copy 2 of 123
Series A.

Contract No. W-7405, eng 26*

ORNL SUMMER SHIELDING SESSION

Gale Young, Leader

DECLASSIFIED Per Letter Instructions Of
AEC-8-30-50

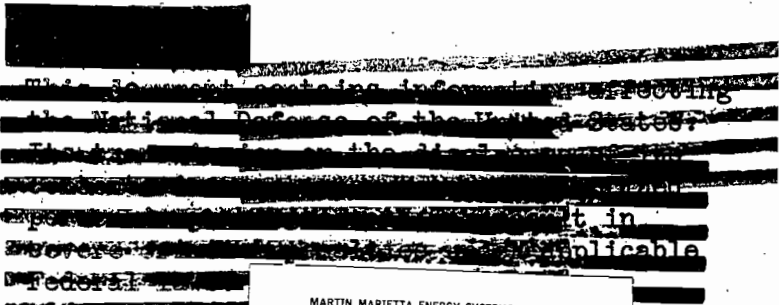
12-19-50 *W.B. Boy*
SUPERVISOR GENERAL FILES

FAST NEUTRON DATA

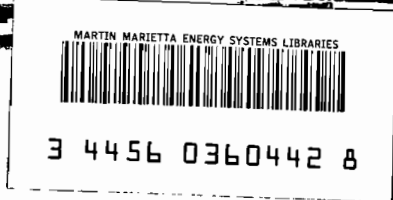
H. Feshbach

DATE ISSUED:
JAN 25 1950

OAK RIDGE NATIONAL LABORATORY
Operated by
CARBIDE AND CARBON CHEMICALS DIVISION
Union Carbide and Carbon Corporation
Post Office Box P
Oak Ridge, Tennessee



* See Explanation on page 3.



This report is one of a series on shielding and represents part of the work of a summer group working principally at Oak Ridge National Laboratory. Participants are drawn from Nuclear Development Associates (Navy contract), NEPA, Bureau of Ships and Bureau of Aeronautics (Navy Department), AEG, RAND, General Electric, Argonne and Oak Ridge National Laboratory

TABLE OF CONTENTS

	Page
I Introduction	5
II Theory	9
A. Resonance Theory	9
B. Non-resonance Theory	19
III Data	29
A. Neutron Sources	29
B. Total Cross-sections	31
C. Inelastic Scattering Cross-sections	50
D. Transport Cross-section	57
E. Particular Elements	58
1. Boron	58
2. Iron	60
3. Tungsten	63
4. Lead	65
IV Curves (Figures No. 1 to No. 29)	68

FAST NEUTRON DATA

H. Feshbach

I. INTRODUCTION

The analysis of shields depends upon accurate neutron data describing the interaction of neutrons with matter. This report is concerned with "fast" neutrons, i.e. neutrons whose energy lies between say 200 k.e.v. and several million electron volts. It includes a compilation and discussion of the available data on substances of interest for the shielding problem. The results of a schematic treatment of the behavior of neutron cross-sections with energy is given and thus provides a method for analyzing the available data and for interpolating and extrapolating for those energy ranges and substances for which data is not available.⁽¹⁾ It should be emphasized that the theory is rather crude and can hardly be expected to yield a detailed explanation of neutron reactions but rather provides a method for making educated guesses.

In addition to the introduction the report consists of three sections. In Section IIA the behavior of neutron cross-sections in the resonance region is discussed. Resonances with fast neutrons are of particular interest for the low mass number shield constituents, as well as for the "magic number" nuclei, such as Pb, which with respect to their interactions with neutrons behave like light elements. Section IIB considers neutron reactions in the non-resonance region, i.e. in the energy region where the energy levels lie so close together and their widths are so large that the erratic ups and downs characteristic of the resonance region are replaced by a smooth, slowly-varying dependence of cross-section on energy. Fortunately the theories for these two energy regions join in the sense that (1), the

(1) The theory employed here is taken largely from Feshbach, Peaslee and Weisskopf, P.R. 71, 145, (1947) and from Feshbach and Weisskopf (in press), and Blatt and Weisskopf (book in preparation). Additional important references are Bethe, Rev. of Mod. Phys. 9, 69, (1937); Wigner, P.R. 70, 15, (1946)

limit of resonance theory as the density of levels increases is the non-resonance theory and (2), the average of the results of resonance theory over many energy levels yields the non-resonance theory. In Section III, the nature of the experimental method for each type of measured cross-section is examined. The available data for each element are discussed and then extrapolated to fill in energy regions in which experiments have not been made.

The cross-sections of interest are listed and discussed below.

A. Total Cross-section σ_t

This is the cross-section determining the attenuation of neutrons through matter.

B. Elastic Scattering Cross-section σ_{el}

σ_{el} determines the manner in which the direction of the incident neutrons is changed upon collision with a nucleus when the target nucleus remains in its ground state after collision. Both the total elastic scattering and the angular distribution will be discussed, the symbol $\sigma_{el}(\theta)$ will be employed for the latter.

C. Inelastic Scattering Cross-section σ_{in}

This cross-section gives the probability that a neutron will excite the target nucleus, the scattered neutron thus having less energy than the incident one. The energy distribution of the scattered neutrons, f , must be known in order to evaluate the slowing down power of the target material. The mechanism here is quite different from that operating in slowing down in a light material, say hydrogen, where the energy loss goes into the kinetic energy of the target nucleus. In inelastic scattering, the residual nucleus being left in an excited state, emits γ -rays which must be included in any discussion of γ -ray attenuation given by a shield.

D. Activation Cross-section σ_{ac}

Low energy neutrons are frequently absorbed, γ -rays being emitted in the process. The process is referred to as the (n,γ) reaction. Activation cross-sections are very small in the fast neutron region. We are, however, interested in the emitted γ -rays which are relevant to the γ -ray attenuation phase of the shielding problem. The residual nucleus is usually radioactive.

E. Absorption Cross-section σ_{ab}

σ_{ab} is the cross-section for the conversion of the incident neutrons into emergent particles which cannot interfere with the incident neutron beam. This occurs because some quantum number of the incident particle such as charge, mass, energy, angular momentum, has been changed by the interaction with the target nucleus. For thermal neutrons on heavy elements, γ -ray emission is much favored over neutron emission. Then $\sigma_{ab} \sim \sigma_{ac}$.

F. Cross-section for Formation of the Compound Nucleus σ_c

This is a measure of the probability that a neutron will enter a nucleus and merge with it to form a compound nucleus. When the compound nucleus decays into the residual nucleus plus emergent particles by principally one route, the cross-section σ_c and the cross-section for this particular event are equal. For example, for thermal neutrons γ -ray emission is dominant so that

$$\sigma_c \simeq \sigma_{ac} .$$

In the high energy region, i.e. energies greater than the first excited level of the target nucleus, formation of the compound nucleus almost always results in neutron emission, with loss of energy. Hence here

$$\sigma_c \simeq \sigma_{in} \simeq \sigma_{ab} .$$

For light elements and relatively low energies elastic scattering dominates so that here

$$(\sigma_{ab} = \sigma_{ac}) \ll \sigma_t ;$$

$\sigma_{ab} \neq \sigma_c$ because of resonance elastic scattering.

G. Transport Cross-section σ_{tr}

The elastic scattering cross-section includes some very small angle scattering. The relative value of such scattering in attenuation is very small indeed since the neutrons move in a nearly forward direction. For high energy neutrons small angle scattering constitutes an important fraction of σ_{el} . A more realistic estimate of the direction changing power of nuclei is provided by σ_{tr} :

$$\sigma_{tr} = \sigma_{el} + \sigma_{in} - 2\pi \int_0^{\pi} \sigma_{el}(\theta) \cos\theta \sin\theta \, d\theta$$

which clearly minimizes small angle scattering.

The transport cross-section weights the differential cross-section $\sigma_{el}(\theta)$ in a way which is appropriate for applications in diffusion theory. It is not clear, however, that the weighting is the best possible for applications in shielding studies. It may be of value in the future to obtain $\sigma_{el}(\theta)$ in detail and to construct other weighted averages.

II. THEORY

The non-resonance theory, as far as it goes, involves only two parameters; the resonance theory requires others in addition. The parameters in common are the nuclear radius R and the average wave number K_0 inside the nucleus of the particle whose total energy is zero. (The zero of energy is taken to be infinitely far away from the target nucleus.) Although both R and K_0 vary with energy, it is assumed that the variation is slow. In the present report K_0 is placed equal to $1.2 \times 10^{13} \text{ cm}^{-1}$. The nuclear radius R is determined by comparison of the non-resonance theory with experiment. It may be expected to fluctuate by as much as 10^{-13} cm about the mean for a given element. Table I gives the nuclear radii evaluated in this fashion, together with the energy region in which the determining experiment was made.

A. Resonance Theory

A description of the resonance energy region requires (a) the behavior of the various cross-sections at and near a resonance, (b) their behavior between resonances and (c) the distance D between resonance energies.

At or near a resonance, the cross-sections are given by the Breit-Wigner formulas. If α represents the quantum numbers associated with the initial state such as the spin of the target nucleus I_1 , the spin of the incident neutron $1/2 \hbar$, etc., and α' the quantum numbers associated with the final state, then the cross-section $\sigma_{\alpha, \alpha'}$ for the formation of state α' from state α is:

$$\sigma_{\alpha, \alpha'} = \frac{2J + 1}{2(2I + 1)} \pi \lambda^2 \frac{\Gamma_{\alpha} \Gamma_{\alpha'}}{(E - E_0)^2 + \Gamma^2/4} \quad (1)$$

TABLE I
NUCLEAR RADII

Element	R x 10 ¹³ cm	Incident Neutron Energy in Mev
Be	2.4	14
B	3.4	14
C	3.8	25
O	4.3	25, .2 to 1.5
Mg	4.5	14
Al	4.6	14, 25
S	4.1	14, 25
Cl	4.7	25
Fe	5.6 4.6	14 .2 to 1.5
Ni	4.6	.2 to 1.5
Cu	5.5	25
Zn	5.9	14
Se	6.3	14
Ag	6.8 6.9 7.5	14 25 .2 to 1.5
Cd	7.2	14
Sn	7.4	14
Au	7.5	14
W	7.8	.2 to 1.5
Hg	8.3	14
Ta	8.4 8.5	25 .2 to 1.5
Pb	7.8	14, .2 to 1.5
Bi	7.9	14, .2 to 1.5
Zr	7.8	.2 to 1.5

where $\lambda =$ neutron wavelength/ 2π , $1/\lambda = k$; $J\hbar =$ total angular momentum of the level of the compound nucleus involved in the resonance; $E_0 =$ resonance energy. $\Gamma_\alpha, \Gamma_{\alpha'}$ are called "widths", Γ , the total width. A relation between Γ_α and Γ exists:

$$\Gamma = \sum_{\alpha'} \Gamma_{\alpha'} . \quad (2)$$

From expression (1) it is possible to obtain the absorption cross-section from state α and the cross-section for the formation of the compound nucleus in state J from state α . The definition of σ_{ab} from state α is

$$\sigma_{ab} = \sum_{\substack{\alpha', \alpha \\ \alpha' \neq \alpha}} \sigma_{\alpha, \alpha'} .$$

Hence

$$\sigma_{ab} = \frac{2J+1}{2(2I+1)} \pi \lambda^2 \frac{\Gamma_\alpha \Gamma_a}{(E-E_0)^2 + \Gamma^2/4} \quad (3)$$

$$\Gamma_a = \Gamma - \Gamma_\alpha .$$

Also since

$$\sigma_c = \sum_{\alpha, \alpha'} \sigma_{\alpha, \alpha'} \quad (4)$$

$$\sigma_c = \frac{2J+1}{2(2I+1)} \pi \lambda^2 \frac{\Gamma_\alpha \Gamma}{(E-E_0)^2 + \Gamma^2/4} . \quad (5)$$

The relations

$$\sigma_{\alpha, \alpha'} = \sigma_c \frac{\Gamma_{\alpha'}}{\Gamma}$$

and

$$\sigma_{ab} = \sigma_c \frac{\Gamma_a}{\Gamma} \quad (6)$$

now follow, and also the interpretation of $\Gamma_{\alpha'}/\Gamma$ as the relative probability for the final state α' . Some obvious features of these cross-sections (3) and

(4) are the maxima at $E = E_0$, e.g.,

$$(\sigma_{ab})_{\max} = 4\pi \lambda^2 \frac{2J+1}{2(2I+1)} \frac{\Gamma_a \Gamma_b}{\Gamma^2}$$

and the symmetry of the energy dependence of the cross-section with respect to E_0 .

The cross-section for elastic scattering, σ_{el} , near resonance is considerably more complex because of the interference between potential and resonance scattering. The formula may be broken up into two parts, one of which corresponds to the emission of neutrons by the compound nucleus which are coherent with the incident neutron beam. We shall call this σ_{co} :

$$\sigma_{co} = \pi \lambda^2 \frac{2J+1}{2(2I+1)} \sum_{\ell} \left| \frac{i\Gamma_{\ell}}{E-E_0 + i\Gamma/2} + (e^{2i\delta_{\ell}} - 1) \right|^2 \quad (7)$$

The resonance term, $i\Gamma_{\ell}/(E-E_0 + i\Gamma/2)$, occurs for those values of ℓ which, for the given target nuclear spin I , may lead to a compound state of spin J . Thus the possible ℓ values vary from $\ell = |J - I|$ to $J + I$. Γ_{ℓ} is a parameter proportional to the relative probability that the component of the incident plane wave of angular momentum $\ell\hbar$ contributes to the process. The remaining term $(e^{2i\delta_{\ell}} - 1)$ is called "potential scattering". The phase δ_{ℓ} is, for neutrons, given by

$$\delta_{\ell} = - \tan^{-1} \frac{N_{\ell+\frac{1}{2}}(x)}{N_{\ell-\frac{1}{2}}(x)} \quad (8)$$

where

$$x = kR = .222 R \sqrt{E(\text{Mev})} \quad (9)$$

if R is expressed in units of 10^{-13} cm and E is the incident neutron energy.

In addition to the coherent cross-section, there is an incoherent cross-section σ_{inc} which contains those transitions in which the angular momentum of the incident neutrons is changed without exciting the target nucleus. Thus

$$\sigma_{inc} = \pi \lambda^2 \frac{2J + 1}{2(2I + 1)} \sum_{\substack{\beta, \beta' \\ \beta \neq \beta'}} \frac{\Gamma_{E, \beta} \Gamma_{E, \beta'}}{(E - E_0)^2 + \Gamma^2/4} \quad (10)$$

where the subscript E denotes the common value of the energy of both the incident and scattered neutron. The subscript β refers to the quantum numbers, other than the energy required to describe the state of the incident neutron plus target nucleus while β' refers to similar quantities for the final state of the system. For incoherent scattering the two groups, β and β' , cannot be identical; this is the meaning of $\beta \neq \beta'$ in the summation above. If the spin of the target nucleus is zero, the subscripts β, β' reduce to l and l' , the orbital angular momentum of the incident and scattered neutrons respectively. The variation in l and l' are given in the discussion immediately below equation (7). The terms included in (10) are part of the absorption cross-section σ_{ab} .

The elastic cross-section is then

$$\sigma_{el} = \sigma_{co} + \sigma_{inc} \quad (11)$$

and the total cross-section

$$\sigma_t = \sigma_{co} + \sigma_{ab}$$

Because of the interference between potential and resonance scattering which appears in (9) the maximum of σ_{el} does not occur at $E = E_0$ and the cross-section is not symmetric about the maximum; indeed it also exhibits a minimum on the low energy side of the maximum. As an example, consider the case of S^{32} for which the resonance occurs at 108 k.e.v., the experimental curve⁽²⁾ is given in Figure 1. For this low energy it may be expected that the J of the level

(2) Adair, Bockelman and Peterson, Phys. Rev. 76, 308, (1949).

in the compound nucleus is $1/2$ since the spin of S^{32} is zero. Then

$$\sigma_{el} = \pi \chi^2 \left\{ \left| \frac{i\Gamma_0}{E-E_0 + i\Gamma/2} + e^{2i\delta_0} - 1 \right|^2 + \left| \frac{i\Gamma_1}{E-E_0 + i\Gamma/2} \right|^2 + 2 \frac{\Gamma_0 \Gamma_1}{(E-E_0)^2 + \Gamma^2/4} \right\}$$

where we have neglected δ_l for $l \gg 1$. For a light element we may assume that this resonance is almost altogether scattering, there being little, if any, activation, so that $\Gamma = \Gamma_0 + \Gamma_1$. Then the maximum occurs at $E \approx E_0 + \frac{\Gamma_0}{2} \tan \delta_0$ while the minimum occurs at $E \approx E_0 - \frac{\Gamma^2}{2\Gamma_0} \cot \delta_0$. As we may see after employment of relations (8) for low energies $\delta_0 \ll 1$, the maximum cross-section is very close to E_0 while the minimum is a finite distance away but only a small fraction of the distance to the next resonances. The cross-section at the maximum is $4\pi \chi^2$ while the cross-section at the minimum is $4\pi \chi^2 \sin^2 \delta_0 \left(1 - \frac{\Gamma_0^2}{\Gamma^2}\right)$. In the case of sulfur the minimum value is mostly due to the other sulfur isotopes and other contaminants.

The structure shown in Figure 1 occurs only if (1) there is sufficient potential scattering to interfere both constructively and destructively with the resonance scattering, and (2) $\sigma_{co} \gg \sigma_{inc}$. In the resonance in oxygen⁽³⁾ at 440 k.e.v., there is essentially no minimum (see Fig. 22). Further analysis reveals that the spin of the level in the compound nucleus is $J = 3/2$, so that $l = 1$ and $l = 2$ neutrons participate. At this energy, their potential scattering for these values of l is too small to give rise to any appreciable destructive interference. The second condition, $\sigma_{co} \gg \sigma_{inc}$, will not be satisfied whenever

(3) Adair, Barschall, Bockelman, and Sala, Phys. Rev. 75, 1124, (1949).

there is a large number of ways in which the level of the compound nucleus may be formed, as will occur, for example, at high neutron energies.

The above formulas (1) - (10) are valid as long as only one level in the compound nucleus, i.e., just one value of J , is involved in the reaction. If, however, the density of levels in the compound nucleus is high, one must sum these formulas over J . It is also possible to obtain, because of the high density of levels, expressions giving the absorption and scattering of a neutron of orbital angular momentum l . When the density is low, it would be difficult to give a simple general formula inasmuch as the result would depend upon what J values were present. For high level density, replacing the widths and resonance energy by averages over J , and finally using

$$\sum_J \frac{2J+1}{2(2I+1)} = 2l+1$$

one obtains for

$$\sigma_{ab}^{(l)} = \pi \chi^2 (2l+1) \frac{\Gamma_{n,l} \Gamma_{a,l}}{(E-\bar{E}_0)^2 + (\Gamma_l/2)^2} \quad \Gamma_l = \Gamma_{n,l} + \Gamma_{a,l} \quad (12)$$

Here $\Gamma_{n,l}$ is a parameter giving the relative probability that a neutron with orbital angular momentum l will be absorbed by the target nucleus, while $\Gamma_{a,l}$ is the relative probability that the residual nucleus is not the same as the target nucleus.

The coherent part of the elastic cross-section may also be found

$$\sigma_{co}^{(l)} = \pi \chi^2 (2l+1) \left| \frac{i \Gamma_{n,l}}{E-\bar{E}_0 + i \Gamma_l/2} + e^{2i\delta_l} - 1 \right|^2 \quad (13)$$

The incoherent term becomes

$$\sigma_{\text{inc}}^{(\ell)} = \pi k^2 (2\ell + 1) \frac{\Gamma_{n,\ell}}{(\mathbb{E} - \mathbb{E}_0)^2 + (\Gamma_{\ell}/2)^2} \sum_{\ell' \neq \ell} A_{\ell', I} \Gamma_{n,\ell'} + (A_{\ell, I} - 1) \Gamma_{n,\ell} \quad (14)$$

where $A_{\ell', I} = \min(2I + 1, 2\ell' + 1)$. The possible values of ℓ' are determined by the fact that the maximum possible change of the target nucleus without its excitation is $2I$, and for the neutron it is 1. Thus the maximum value of ℓ' is $\ell + 2I + 1$. The elastic cross-section for " ℓ " neutrons is given by $\sigma_{\text{co}}^{(\ell)} + \sigma_{\text{inc}}^{(\ell)}$, the total cross-section $\sigma_t^{(\ell)}$ is $\sigma_{\text{ab}}^{(\ell)} + \sigma_{\text{co}}^{(\ell)}$. Finally the cross-sections for the entire incident plane wave are given by:

$$\sigma_{\text{ab}} = \sum_{\ell} \sigma_{\text{ab}}^{(\ell)} \quad (15a)$$

$$\sigma_t = \sum_{\ell} \sigma_t^{(\ell)} \quad (15b)$$

The energy dependence of cross-sections $\sigma_{\text{ab}}^{(\ell)}$ and $\sigma_{\text{el}}^{(\ell)}$ is very similar to that given in (3) and (11) and needs no further elaboration.

Application of the above formulas involve the parameters R and the widths Γ_{α} . The widths are not independent of the energy. However, if the resonance energy is sufficiently high and the resonance sufficiently narrow, the variation of the widths over the resonance is small. The variation of width with energy for the neutron widths $\Gamma_{n,\ell}$ have been estimated as:

$$\begin{aligned} \Gamma_{n,\ell} &\approx \frac{2x}{X_0} \frac{1}{|v_{\ell}|^2} \frac{D_{\ell}}{\pi} \\ |v_{\ell}| &= \left| \left(\frac{\pi x}{2} \right)^{\frac{1}{2}} H_{\ell+\frac{1}{2}}^{(1)}(x) \right| \\ X_0 &= K_0 R \end{aligned} \quad (16)$$

In a more precise formula K_0 is replaced by

$$K = \sqrt{K_0^2 + k^2}$$

where $H_{\ell+1/2}^{(1)}$ are Hankel functions and have been tabulated.⁽⁴⁾ The parameter D_ℓ is the energy distance between levels of the compound nucleus which are formed when the target nucleus absorbs an " ℓ " neutron. It must be determined from experiment although estimates may be made from statistical theory to be discussed later on. From (16) we see that $\Gamma_{n,\ell}/D$ depends only upon the parameter x , regardless of the nucleus involved. Relation (16) has been found to hold in order of magnitude for $\ell = 0$ neutrons.⁽⁵⁾

The total neutron width Γ_n is

$$\Gamma_n = \sum_{\ell} (2\ell + 1) \Gamma_n^{(\ell)}. \quad (17)$$

The factor $(2\ell+1)$ is approximate. For sufficiently high neutron energies it seems reasonable to assume that D_ℓ is independent of ℓ :

$$D_\ell \approx D.$$

Then

$$\Gamma_n \approx \frac{2x}{k_0} \frac{D}{\pi} \sum_{\ell} \frac{2\ell + 1}{|v_\ell|^2} = \Gamma_n^{(0)} \sum_{\ell} \frac{2\ell + 1}{|v_\ell|^2}. \quad (18)$$

The function $\sum_{\ell} (2\ell + 1) \frac{x}{|v_\ell|^2}$ is plotted in Figure 2 where it is seen to be one which increases rapidly with x . Formula (18) will prove to be particularly useful in discussing inelastic scattering and, in addition, the deviations to be expected from the average over resonances obtained from the non-resonance theory to be discussed in the next section.

We now turn to the other two matters pertinent to the resonance region, the energy distance D between resonances and the behavior of the cross-section between resonances. For D we shall employ an empirical formula whose form is

⁽⁴⁾ Morse, Lowan, Feshbach and Lax, issued by NDRC, Div. 6.

⁽⁵⁾ Wigner, Am. J. Phys. 17, 107, (1949).

suggested by the free particle model*:

$$D \approx C e^{-\sqrt{AE/5}} \quad (19)$$

where \mathcal{E} is the excitation energy in Mev available to the compound nucleus, A the mass number, C a constant. The excitation energy will contain the incident kinetic energy E of the neutron together with the binding energy E_b available once the compound nucleus is formed. It is clear from (19) that D (and therefore Γ_n) will depend very strongly upon E_b . Thus both light nuclei and "magic number" nuclei have large D values, although for different reasons. For light nuclei, D is large because A is small, while for magic number nuclei D is large since \mathcal{E} is comparatively small. From (18) it follows that these nuclei will have comparatively large values of Γ_n . Hence most resonances in these nuclei are scattering resonances, and correspondingly the activation cross-section is always very small.

For low lying levels of light nuclei which are revealed in inelastic neutron scattering experiments, (d,p) reactions, and in the γ -ray spectrum emitted in an (n, γ) process, D is often rather constant and independent of the energy.

The behavior of the cross-sections between resonances may be obtained from the above formulas by the approximate procedure of simply omitting the resonance terms. Hence

$$\sigma_{ab} \ll \sigma_t$$

$$\sigma_{el} \approx \sigma_t = 4\pi \chi^2 \sum_{\ell} (2\ell + 1) \sin^2 \delta_{\ell} \quad (20)$$

* Actually the free particle model gives the form $D \sim \mathcal{E}^4 e^{-\sqrt{A} \mathcal{E}/\text{const}}$. We do not include this factor, \mathcal{E}^4 , inasmuch as (1) it affects D in a weak fashion so that it is difficult to check it experimentally, and (2) the derivation involves so many weak links that it seems hardly likely that the proper exponent for \mathcal{E} could have been determined.

This is called repulsive sphere scattering since it is the scattering which results if the neutron wave function must go to zero at the surface of the nucleus. Formulas (20) are approximate since $\sigma_{ab} \neq 0$ between resonances. However, if $D \gg \Gamma$, the value of σ_{ab} here should be very small. Cross-section (20) is given in Figure 3. At zero energy it has the value $4\pi R^2$ and monotonically approaches the asymptotic value of $2\pi R^2$ at infinite energy. It is important to note that the deviations from the asymptotic value are fairly large at even large values of x . In this region $\sigma_t \sim 2\pi R^2(1 + 1/x)^2$ so that the approach to $2\pi R^2$ is very gradual.

We shall close this section with some remarks on the application of the above results to fast neutron data. For the energy region in question resonances will appear in light nuclei and also for the so-called "magic number" nuclei which, as has been pointed out above, behave very much like light nuclei. Resonances for fast neutrons are scattering resonances. They may exhibit the structure illustrated in Figure 1 if they occur at low enough energy. We estimate that the minima which give rise to "windows" in the energy spectrum will not occur for neutron energies larger than about 1 Mev for light elements and about 1/2 Mev for the magic number heavy nuclei.

B. Non-Resonance Region

As the energy of the incident neutron increases, the width Γ associated with the levels increases rapidly with respect to the level distance D (see Figure 2 for Γ_n variation) so that levels begin to overlap and the irregular behavior of the cross-sections with energy which is so characteristic at lower energies disappears. The prediction of the consequent smooth energy dependence will form the subject of this section. We shall also find useful the result that the formulas obtained apply as well in the resonance region if they are interpreted as average cross-sections averaged over an energy region containing several resonances.

The theory employed here is based on the theoretical expectation and the experimental evidence that, in this energy region, if a neutron has combined with the target nucleus to form a compound nucleus the probability for its re-emission with all of its original quantum numbers unchanged is negligible. Rather, these neutrons may be re-emitted with either their energy changed, i.e. inelastic scattering; their angular momentum may be changed; or both. The neutron may not be re-emitted at all, but rather some other particle, etc. Thus the target nucleus acts as a sink for neutrons labelled by a specific set of quantum numbers. This statement may be mathematically formulated. One may then obtain the cross-section σ_{tot} and σ_c . The elastic cross-section may be obtained only if it is assumed that if the neutron is re-emitted, its energy is almost certainly not the same as that of the incident neutron. Thus all of the elastic scattering will be due to the repulsive sphere scattering plus the shadow scattering associated with the formation of the compound nucleus. For sufficiently high energy this will be true. Then $\sigma_{el} = \sigma_t - \sigma_c$. We shall later in this section extend the theory so as to permit the evaluation of "average" inelastic cross-section and the average of the incoherent elastic scattering.

The results of the theory are summarized in Figures 3, and 4, where the cross-section for σ_t , σ_c , and σ_{tr} are plotted for various values of X_0 . We have included in the σ_t curve the comparison curve $2\pi R^2(1 + 1/x)^2$ which gives the high energy behavior of the σ_t curves. The σ_{tr} curves tend asymptotically to πR^2 for large x . For small x they become identical with the σ_t curves. The calculation of σ_{tr} involves the assumption that that part of the process which involves the formation of the compound nucleus leads almost always to isotropic neutron emission. At small values of x

$$\sigma_c \xrightarrow{x \rightarrow 0} \pi R^2 \left[\frac{1}{x^2} \frac{2\pi \Gamma_{n,0}}{D} \right] = \pi R^2 \left[\frac{4}{xX_0} \right]; \quad (21)$$

also

$$\sigma_t \xrightarrow{x \rightarrow 0} \sigma_c. \quad (22)$$

For the larger values of X_0 , the σ_c curve shows a minimum in the neighborhood of $x = 1.5$ corresponding to energies of 1 Mev and 1/2 Mev for $X_0 = 8$ and 11 respectively. At larger values of x , the σ_c curve for $X_0 = 8$ is almost constant with $\sigma_c/\pi R^2 = 1.2$; while for $X_0 = 11$, $\sigma_c/\pi R^2 = 1.05$ is accurate to within 10%. The $X_0 = 5$ curve is monotonic and more rapidly varying than the other curves. Between $x = 3$ and 12, $\sigma_c/\pi R^2 = 1.35$ is accurate to within 10%. This approximate constancy permits the evaluation of experiments involving neutron beams whose energy distribution is broad.

The non-resonance theory may also be used to estimate the cross-section for inelastic scattering and the energy distribution of the emitted particles. Let the wave number of the incident neutron be $k(x = kR)$, its energy E , and let the wave number of the emitted neutron leaving the target nucleus in the i^{th} excited state of energy E_i be $k_i(x_i = k_i R)$. Let the corresponding neutron widths be $\Gamma_n(x)$ and $\Gamma_n(x_i)$. Then approximately

$$\sigma_{in} = \sigma_c \frac{\sum_i \Gamma_n(x_i)}{\Gamma_n(x) + \sum_i \Gamma_n(x_i)} = \sigma_c \left(1 + \frac{\Gamma_n(x)}{\sum_i \Gamma_n(x_i)} \right)^{-1} \quad (23)$$

where it has been assumed that the only important processes are those of neutron emission, which is reasonably accurate for fast incident neutrons. The summation in (23) includes, of course, only those levels for which E_i is less than the incident neutron energy. The fractional number of particles f_j having an energy corresponding to $x_j = .222 R \sqrt{E-E_j}$ is

$$f_j = \frac{\Gamma_n(x_j)}{\sum_i \Gamma_n(x_i)} \quad (24)$$

From the estimate of Γ_n/D given in Figure 2, (23) and (24) may be evaluated if the energy levels of the target nucleus are known. Note that D, which is the distance between levels in the compound nucleus, is a common factor of both numerator and denominator in (23) and (24) and therefore need not be known.

If, as is common at present, the level scheme is not known, an estimate of (23) and (24) may be obtained. This will also furnish a rule of thumb which will prove useful even when complete information is available. To obtain the estimate we first assume that the levels are distributed continuously so that

$$\sum \Gamma_n(x_1) = \int_{E_0}^E \rho(E_1) \Gamma_n(x_1) dE_1 \quad (25)$$

where $\rho(E_1)$ is the density of levels of the target nucleus. E_0 is the energy of its first excited level. Equation (24) becomes

$$f_j = \frac{\Gamma_n(x_j)}{\int_{E_0}^E \rho(E_1) \Gamma_n(x_1) dE_1} \quad (26)$$

and $\rho_j(E_j) f_j dE_j$ is the fractional number of particles in dE_j at E_j .

Before proceeding, it is useful to have some approximate analytic form for Γ_n/D . Statistical theory suggests $\Gamma_n/D \sim x^2$, while at higher energies ($x \rightarrow \infty$) $\Gamma_n/D \sim x^3$. Upon fitting the curve for Γ_n/D , it was found that x^2 was a good fit up to $x = 2$, but that for larger values of x it fell below the correct value as expected. Up to $x = 4$, an excellent fit is obtained with $x(1 + x + .9x^2)$. Thus

$$\frac{\pi X_0}{2} \frac{\Gamma_n}{D} \simeq 3x^2 \quad \text{Approximation A} \quad (27a)$$

$$\simeq x(1 + x + .9x^2) \quad \text{Approximation B} \quad (27b)$$

In Table 2 these are compared with values computed directly from (18).

Table 2

x	Approximation A	From Eq. 18	Approximation B
0	0	0	0
.5	.75	.96	.86
1	3.0	2.91	2.9
2	12	13.0	13
3	27	34.1	36
4	48	70.5	78

We shall now evaluate (25) and (26) for two cases. In case (1) ρ is roughly independent of energy, so that ρ may be replaced by an average value $\bar{\rho} = 1/\bar{D}$. This should apply when low lying levels of light or magic number nuclei are excited. Then

$$\frac{\pi X_0}{2D} \sum_1 \Gamma_n(x_1) = \frac{3}{2} \bar{\rho} x_0^2 (E-E_0) \quad \text{in approximation A} \quad (28a)$$

or

$$= \bar{\rho} x_0 (E-E_0) \left\{ \frac{2}{3} + \frac{1}{2} x_0 + .36 x_0^2 \right\} \quad \text{in approximation B} \quad (28b)$$

where $x_0 = .222 R \sqrt{E-E_0}$. Note that D in the above formula is the level distance in the compound nucleus while $\bar{\rho} = 1/\bar{D}$ is the average level density in the final nucleus.

Consequently,

$$\sigma_{in} = \sigma_c \left[1 + \frac{2E\bar{D}}{(E-E_0)^2} \right]^{-1} \quad \text{in approximation A} \quad (29a)$$

and

$$\sigma_{in} = \sigma_c \left[1 + \frac{E^{1/2}\bar{D}}{(E-E_0)^{3/2}} \frac{(1+x+.9x^2)}{\frac{2}{3} + \frac{1}{2}x_0 + .36x_0^2} \right]^{-1} \quad \text{in approximation B} \quad (29b)$$

It is clear from these formulas that

$$\sigma_{in} \approx \sigma_c \quad \text{if } (E-E_0)^2 \gg \bar{D}E. \quad (30)$$

The energy distribution is obtained from (26). Let $\xi_j = E-E_j$ be the energy of the emitted neutrons

$$f_j = \frac{2 \xi_j \bar{D}}{\xi_0^2} \quad (31a)$$

$$f_j = \frac{\xi_j^{1/2} \bar{D}}{\xi_0^{3/2}} \frac{1 + x_j + .9x_j^2}{\frac{2}{3} + \frac{x_0}{2} + .36x_0^2} \quad (31b)$$

We turn now to case (2). Here ρ is given by the statistical theory:

$$\rho(E) = C^{-1} e^{\sqrt{\alpha E}} \quad (32)$$

In equation (19) α was placed equal to $A/5$ if E is in Mev. Formula (28) should apply in this context to heavy nuclei which have low closely spaced levels. We find that $(\pi X_0/2D) \sum_1 \Gamma_n(x_1)$ is proportional to

$$12E\rho(E)x^2 \frac{(\alpha E - 3(\alpha E)^{1/2} + 3)}{\alpha^2 E^2} \quad \text{in approximation A} \quad (33a)$$

and proportional to

$$2xE\rho(E) \left[\sqrt{\frac{\pi}{2}} \frac{1}{(\alpha E)^{3/4}} + \frac{2x}{\alpha E} + \sqrt{\pi} \frac{x^2}{(\alpha E)^{5/4}} \right] \quad \text{in approximation B} \quad (33b)$$

under the addition approximations $e^{-\sqrt{\alpha E}} \ll 1$ and $E \gg E_0$. Then in approximation A

$$\sigma_{in} = \sigma_c \left[1 + \frac{\alpha D(E) (\alpha E)}{4 [\alpha E - 3(\alpha E)^{1/2} + 3]} \right]^{-1} \quad (34a)$$

while

$$\sigma_{in} = \sigma_c \left[1 + \frac{\alpha D(E) (\alpha E)^{1/4}}{2 \left[\sqrt{\frac{\pi}{2}} (\alpha E)^{1/2} + 2x(\alpha E)^{1/4} + \sqrt{\pi x^2} \right]} \right]^{-1} \quad (34b)$$

in approximation B.

The rapidity with which $\sigma_{in} \rightarrow \sigma_c$ as the energy increases is indicated in Figure 5 where we have plotted

$$\frac{f_A}{C\alpha} = \frac{1}{4} e^{-\sqrt{\alpha E}} (\alpha E) \left[\alpha E - 3(\alpha E)^{1/2} + 3 \right]^{-1}$$

where C is the level distance for zero excitation energy. We repeat that equation (34) is valid only when

$$e^{-\sqrt{\alpha E}} \ll 1 \quad \text{and} \quad E \gg E_0. \quad (35)$$

In applying (34) it is necessary to determine the parameters C and α from whatever is known about the density of levels in the target nucleus. Relation (16) is often valuable in this connection. In the absence of any experimental information, the empirical relation $\alpha = A/5$ is useful.

The energy distribution is given for approximation A by

$$\rho_j f_j = \alpha^2 \xi_j e^{-\left[\sqrt{\alpha E} - \sqrt{\alpha(E-\xi_j)} \right]} \frac{1}{4 \left[\alpha E - 3(\alpha E)^{1/2} + 3 \right]} \quad (36a)$$

where ξ_j is the energy of the emerging neutrons, $E - E_j = \xi_j$. Equation (36a) is already normalized, but the dependence on ξ_j is clearer if the normalizing factor is dropped:

$$\rho_j f_j \sim \xi_j e^{-\left[\sqrt{\alpha E} - \sqrt{\alpha(E-\xi_j)} \right]} \quad (37a)$$

In the event that $\epsilon_j \ll E$, the exponent may be expanded so that

$$\rho_j f_j \sim \epsilon_j e^{-\epsilon_j/\tau} \quad \epsilon_j \ll E \quad (38)$$

where τ , "the nuclear temperature" is

$$\tau = 2 \sqrt{E/\alpha} \quad (39)$$

Formula (37) was originally derived by Weisskopf in the so-called "evaporation" theory of nuclear reactions. We see that its validity is restricted to the lower energy domain. The more accurate distribution given by (37) does not fall off as rapidly as approximate (38).

Approximation B yields formulas which are somewhat more accurate at higher neutron energies. From $\rho_j f_j \sim \Gamma(x_j) e^{-[\sqrt{\alpha E} - \sqrt{\alpha(E-\epsilon_j)}]}$ one finds:

$$\rho_j f_j \sim (x_j + x_j^2 + .9x_j^3) e^{-[\sqrt{\alpha E} - \sqrt{\alpha(E-\epsilon_j)}]} \quad (37b)$$

In passing note that the cross-section for incoherent elastic scattering σ_{inc} is given by

$$\sigma_{inc} = \sigma_c - \sigma_{in}$$

We conclude this section on non-resonance theory by recalling that it applies as well if averages are taken over an energy range large enough to contain several resonances. To complete this picture it is necessary to discuss the deviations from the average. An estimate may be readily made in the energy region $E \sim 1$ Mev, for here the effects of the interference between potential and resonance scattering are no longer an important fraction of the total cross-section. In other words, above 1 Mev it is expected that there should be no energy "window" in σ_t . In that event

$$(\sigma_t)_{min} \simeq \sigma_0 \quad (40)$$

where σ_0 is the infinitely repulsive sphere scattering (Fig. 3). The maximum cross-section is computed by comparing it with the average. Then

$$(\sigma_t)_{\max} - \sigma_0 \leq \frac{2}{\pi} \frac{D}{\Gamma} (\sigma_t - \sigma_0).$$

The choice of the constant $2/\pi$ is based on results for $D \gg \Gamma$, i.e. when the resonances are widely spaced. Moreover an average level distance D is used. Actually the level distance between individual levels fluctuates around this average. This fluctuation would result in a fluctuation in the energy dependence of σ_t which is not included in the above formula. This effect may be included by increasing the constant $2/\pi$. It is found that the constant 2 is more realistic. Hence

$$(\sigma_t)_{\max} - \sigma_0 \simeq 2 \frac{D}{\Gamma} (\sigma_t - \sigma_0) . \quad (41)$$

We have discussed the evaluation of Γ/D above so that it becomes possible to determine $(\sigma_t)_{\max}$.

We may also employ the above analysis to determine the energy at which the fluctuations and therefore the resonances have mostly disappeared. In (41), we equate $\sigma_t = (\sigma_t)_{\max}$ to obtain the equation $\Gamma = 2D$. This equation may be solved for the energy E_c required. Precise solution of this equation can be obtained only if sufficient information about the levels of the compound nucleus is available. An upper bound may be obtained by assuming that most of the scattering is elastic. Then $\Gamma \sim \Gamma_n$. Employing the statistical approximation (27a) it is easy to solve for E_c :

$$E_c \leq \frac{20\pi}{3} \frac{K_0}{R} = \frac{8\pi}{R} . \quad (42)$$

Energy is expressed in Mev, and length in 10^{-13} cm. Formula (42) should be a fairly good estimate if the excited levels of the target nucleus are high as they would be in a light nucleus. In oxygen, for example, we find $E_c \leq 5.8$ Mev.

A lower limit to the critical energy may be obtained if it is assumed that inelastic scattering is dominant at $E = E_c$. Then $\Gamma = \sum_n \Gamma_n(x_1)$. Employing the result obtained by statistical theory (33a), we find E_c is a solution of

$$\frac{3x^2}{\pi X_0 \alpha C} = \frac{f}{\alpha C} \quad (43)$$

where $(f/\alpha C)$ is a tabulated function of $\sqrt{\alpha E}$ given in Figure 5. As an example let

$$\alpha = 40$$

$$C = .1 \text{ Mev}$$

$$R = 8$$

$$X_0 = 9.6$$

$$\text{Then } E_c \gg .3 \text{ Mev.}$$

Equation 43 should be applied to heavy nuclei where one may expect many low lying levels and apply (42) to light nuclei whose first excited level occurs at a rather large ($E_c \gtrsim E_0$) energy value.

III. DATA

A. Neutron Sources

The neutron sources employed in fast neutron experiments have been described in two reports: Hanson and Taschek, "Monoenergetic Neutrons from Charged Particle Reactions", preliminary report No. 4, Nuclear Science Series; and A. Wattenberg, "Photo-neutron Sources", preliminary report No. 6. We shall discuss here only those points which are pertinent to the analysis of the data given in this report.

1. Bombarding particles either H^1 , H^2 , or He^4 .

a) $Li^7(p,n)Be^7$. The threshold for this reaction is 1.88 Mev. The neutrons produced are monochromatic for a given angle with respect to the initial proton direction. This source has been utilized at Los Alamos and later by Barschall's group at the University of Wisconsin and by Williams and his co-workers at the University of Minnesota. The neutron energy range covered in their research extends from about 50 k.e.v. to 1.5 Mev. Extension to higher energies is limited by the maximum energy of the protons which are produced by the Van de Graaff generators available at each laboratory. Excellent energy resolution is possible and has been employed in some of the experiments.

b) $D(d,n)He^3$. This reaction is exoergic, the Q value being 3.31 Mev. The neutron energies are monochromatic for a given angle. The neutron energies available for incident deuteron of 4 Mev extends from 1.65 Mev in 180° direction to 7.45 Mev in the zero degree direction. This neutron source was very popular prior to World War II because it provided neutrons of high energy for incident deuterons whose energy was of the order of a few hundred kilovolts.

This energy source has been utilized by Zinn, Seeley, and Cohen (2.85 and 2.46 Mev), Kikuchi and Aoki (2.46 Mev), Aoki (2.2 to 2.8 Mev), McPhail (2.3 Mev - 2.8 Mev) and Nuckolls, Bailey, Bennett, Bergstrahl, Richards and Williams (2 - 6 Mev).

c) $\text{Li}^7(\text{d},\text{n})\text{Be}^8$. In this reaction, the neutrons produced at a given angle and deuteron energy are not monochromatic. However, by using threshold detectors it is possible to isolate the upper end of the neutron spectrum. For example, Amaldi, Bocciarelli, Cacciaputo, Trabacchi, and Soltan use a $\text{Cu}^{63}(\text{n},2\text{n})\text{Cu}^{62}$ detector to isolate the 14 Mev group. Sherr uses a similar carbon reaction, $\text{C}^{12}(\text{n},2\text{n})\text{C}^{11}$ with a 21 Mev threshold, to isolate a neutron group running from 21 to 25.4 Mev.

d) $\text{C}^{12}(\text{d},\text{n})\text{N}^{13}$. This reaction yields monochromatic neutrons. Since the Q value is -.26 Mev, neutrons in the 0.5 to 2 Mev range may be obtained with deuteron energies that are considerably lower than those required in the $\text{Li}^7(\text{p},\text{n})\text{Be}^7$ reaction. For example, if the deuteron energy is 1.5 Mev, neutrons from about 1.5 Mev at 0° to .75 Mev (180°) are made available. This reaction was utilized by Nuckolls et al. in measuring the oxygen cross-section.

e) $\text{H}^3(\text{d},\text{n})\text{He}^4$. The Q for this reaction is 17.6 Mev. It yields monoenergetic neutrons whose energy for an incident deuteron energy of 2.5 Mev lies between 12 and 18 Mev. In this report experiments on inelastic scattering by Gittings, Everhart, and Barschall, and by Phillips and Davis employ 14 Mev neutrons obtained from this reaction.

2. Photoneutron Sources

Fields, Russell, Sachs, and Wattenberg employ neutrons generated by the photodisintegration of H^2 and Be^9 . The photon energy must be at least 2.23 Mev and 1.63 Mev respectively. The required γ -rays are produced in the disintegration of artificially radioactive substances which may be obtained in some quantity from the pile. The principal advantage of this type of source is the relatively monoenergetic character of the emitted neutrons. Actually absorption and scattering in the γ -ray source gives the neutrons an energy spread of about 25% of

the neutron energy. The low neutron intensity and the high γ -ray background give rise to the main experimental difficulties. We list the neutron energies utilized by Fields et al.

Table 3

Photoneutron Energies

Source	Neutron Energy	Energy of γ -rays as deduced from neutron energies
Sb+Be	.025 Mev	1.66 Mev
Ga+D ₂ O	.13	2.36
Mn+Be	.14	1.77
Na+D ₂ O	.22	2.45
La+Be	.62	2.25
Na+Be	.83	2.46

B. Total Cross-section*

A list of the elements for which σ_t for fast neutrons has been measured together with references is given in the table below. The work of Barschall and his collaborators, and those of Williams et al are too detailed to permit numerical quotation. It is included in graphical form (Figs. 6 - 13). In this report we have concentrated upon B, O, Fe, W, Pb, and these are discussed later. The data taken below 1.5 Mev by Barschall et al, Williams et al, and Fields et al are in excellent agreement except for the case of boron where Fields' points lie

* Authors of papers will be referred to by giving a list of the first letter in the names of the contributing authors whenever this is possible without confusion. For example, Barschall, Battat and Bright will be referred to as BBB. A list of the abbreviations is given in Table IV.

well above those of BBB. The data taken in the 2 - 3 Mev region employing D-D neutrons often disagree violently quantitatively, though in their qualitative energy dependence they agree. Part of these discrepancies are undoubtedly due to the strong resonances which are still present at these energies for the lighter elements. Agreement between non-resonance theory and experiments is excellent for the cases discussed in detail in this report together with several others discussed in Feshbach and Weisskopf. Three elements do not seem to have the behavior predicted by theory, σ_t being almost constant with energy. These are Sb, I, and In.

Examination of the data reveals that there are few experiments in the gap between 1.5 and 2.2 Mev. The experiments above 2.2 Mev are not in agreement with each other and are not sufficient to yield the detailed structure of the cross-section dependence on energy. Above 3 Mev there are very few measurements indeed. There are measurements on oxygen taken by NBBBRW up to 6 Mev, some at 14 Mev by ABCT, and finally several more at 25 Mev taken by Sherr.

Most of these data are included in the review article by Goldamith, Ibsen, and Feld (Rev. Mod. Phys. 19, 259, 1947) where they are presented in graphical form.

Table 4

References Quoted on Total Cross-section Data

A	Aoki	Proc. Phys. Math. Soc. of Japan, <u>21</u> , 232, 1939
AABT	Ageno, Amaldi, Bocciarelli, Trabocchi	Phys. Rev. <u>71</u> , 20, 1947
ABBS	Adair, Barschall, Bockelman and Sala	Phys. Rev. <u>75</u> , 1124, 1949
ABP	Adair, Bockelman, Peterson	Phys. Rev. <u>76</u> , 308, 1949
ABCT	Amaldi, Bocciarelli, Caciapuoto, Trabacchi	Nuovo Cimento <u>3</u> , 203, 1946
BBB	Barschall, Battat, and Bright	Phys. Rev. <u>70</u> , 458, 1946.
BBS	Barschall, Bockelman, and Seagondollar	Phys. Rev. <u>73</u> , 659, 1948
BBBNRW	Bailey, Bennett, Bergstrahl, Nuckolls, Richards and Williams	Phys. Rev. <u>70</u> , 583, 1946
BM	Bretscher and Murrell -- quoted by Goldsmith, Ibser and Feld	
BPAB	Bockelman, Peterson, Adair, Barschall	Phys. Rev. <u>76</u> , 277, 1949
B....	Barschall et al	Unpublished
F	Frisch, D. H.	Phys. Rev. <u>70</u> , 589, 1946
GS	Good and Scharff-Goldhaber	Phys. Rev. <u>59</u> , 917, 1941
KA	Kikuchi and Aoki	Proc. Phys. Math. Soc. of Japan, <u>21</u> , 75, 1939
M	McPhail	Phys. Rev. <u>57</u> , 669, 1940
NBBERW	Nuckolls, Bailey, Bennett, Bergstrahl, Richards and Williams	Phys. Rev. <u>70</u> , 805, 1946.
S	Sherr	Phys. Rev. <u>68</u> , 240, 1945.
SB	Seagondollar and Barschall	Phys. Rev. <u>72</u> , 439, 1947
W....	Williams et al	Unpublished
Wa	Wattenberg	Phys. Rev. <u>71</u> , 497, 1947
ZSC	Zinn, Seeley and Cohen	Phys. Rev. <u>56</u> , 260, 1939

Table 5

Table of Elements and References for Total Cross-sections

Element	Reference
B	FRSW, BBB, ABCT, A, KA
C	Wa, F, EM, BBBNRW, A, M, AABT, S, KA
N	F, A, M, ZSC, KA
O	FRSW, NBBBRW, A, ZSC, S, W..., ABBS, KA
F	FRSW, A, KA
Ne	
Na	FRSW, A, M, ZSC, ABBS, KA
Mg	FRSW, A, ABCT, KA
Al	SB, FRSW, GS, M, A, ZSC, ABCT, S, KA
Si	KA
P	FRSW, A, KA
S	FRSW, A, ZSC, ABCT, ABP, KA
Cl	S, KA
A	
K	FRSW, A, ZSC, KA
Ca	ABBS, KA
Sc	
Ti	KA
V	
Cr	KA
Mn	KA
Fe	A, ZSC, ABCT, FRSW, BBS, KA
Co	KA
Ni	FRSW, A, ABCT, BBS, KA

cont'd

Table 5 (cont'd)

Element	Reference
Cu	FRSW, GS, A, ZSC, AABT, S, KA
Zn	ZSC, ABCT, KA
Ga	
Ge	
As	KA
Se	ABCT
Br	KA
Rb	
Sr	KA
Y	
Zr	BPAB
Cb	
Mo	
Tc	
Ru	
Rh	
Pd	
Ag	FRSW, A, ABCT, BPAB, S, KA
Cd	ABCT, KA
In	
Sn	FRSW, A, ZSC, ABCT, KA
Sb	FRSW, A, ABCT, BPAB, KA
Te	
I	FRSW, A, BPAB, KA
Xe	
Cs	

cont'd.

Table 5 (cont'd)

Element	Reference
Ba	KA
La	
Ce	
Pr	
Nd	
Pm	
Sm	
Eu	
Gd	
Tb	
Dy	
Ho	
Er	
Tm	
Yb	
Lu	
Hf	
Ta	BPAB
W	FRSW, A, B....., KA
Re	
Os	
Ir	
Pt	
Au	ABCT
Hg	ABCT, S, KA

cont'd

Table 5 (cont'd)

Element	Reference
Tl	
Pb	FRSW, GS, A, ZSC, ABCT, BM, BPAB, KA
Bi	FRSW, A, ABCT, BBS, KA
Np ²³⁷	K

Agno, Amaldi, Bocciarelli, Trabacchi

σ_t on carbon

Energy	σ_t (barns)	Source
4.1 Mev	1.99	(D + Be)
12.5	1.40	(D + B)
13.5	1.23	(D + Li)

Amaldi, Bocciarelli, Caciapuoto, Trabacchi

(Li + D neutrons)
Neutron energy 14 Mev

Element	σ_t (barns)
Be	.65
B	1.16
Mg	1.83
Al	1.92
S	1.58

cont'd

Amaldi Bocciarelli, Caciapuoto, Trabacchi (cont'd)

Element	σ_t (barns)
Fe	2.75
Zn	3.03
Se	3.35
Ag	3.82
Cd	4.25
Sn	4.52
Sb	4.35
Au	4.68
Hg	5.64
Pb	5.05
Bi	5.17

Aoki (D + D) neutrons

σ_t (barns)

Energy (Mev) →	2.85	2.70	2.55	2.38	2.2
B	1.95		2.27		1.86
C	1.95	1.69	1.64	1.52	1.56
N	2.12	...	1.83		2.35
O	1.29		1.14		1.23
F	1.73		2.10		1.95
Na	2.80		3.18		3.09
Mg	2.00		1.94		2.02

cont'd

Aoki (cont'd)

Energy (Mev) →	2.85	2.70	2.55	2.38	2.2
Al	2.35	2.56	2.83	2.45	2.66
Si	2.25	2.43	2.88	2.25	2.29
P	3.05	3.02	2.93	2.71	3.12
S	2.68	2.66	2.50	2.52	2.03
Cl	2.84		2.66		2.67
K	3.67		3.66		3.62
Ti	2.00		2.11		1.85
Cr	3.29		3.08		3.02
Mn	3.31		3.30		3.08
Fe	2.9	2.84	3.02	2.64	2.55
Ni	2.78		2.64		2.48
Cu	2.68	2.71	2.59	2.61	2.50
Zn	2.72		2.74		2.62
Ag	3.57		3.73		3.81
Cd	3.75		4.14		4.03
Sn	3.82	3.80	3.90	4.01	4.15
Sb	4.50	4.62	4.71	4.70	4.80
I	4.75		4.95		4.88
Ba	6.51		6.89		6.69
W	5.94		6.10		5.77
Hg	5.27		5.16		4.75
Pb	5.46	5.19	5.24	5.38	4.82
Bi	6.01	5.79	5.64	5.52	5.35

Bailey, Bennett, Bergstrahl, Nuckolls, Richards, Williams

(Li + p, C¹² + D, D + D neutrons)

σ_t (barns) on Carbon

Neutron Energy	σ_t
.35 Mev	3.15
.46	3.15
.72	2.49
.97	2.40
1.0 ± .1	2.38
1.6	1.90
2.0	1.63
2.6	1.60
2.85	1.57
3.0	1.59
3.25	1.69
3.5	2.39
3.75	2.43
4.0	1.85
4.25	2.16
4.5	1.93
4.75	1.60
5.0	1.18
5.5	1.07
6.0	1.11

Barschall, Battat, Bright

(Li + p neutrons, D + D neutrons)

E_n	σ_t (barns)		
	Normal	B^{11}	B^{10}
.2	3.5	3.4	4.1
.6	2.4	2.2	3.5
.8	1.8	1.6	2.6
1.0	1.6	1.4	2.3
1.2	2.0	2.2	1.5
1.5	1.9	1.9	1.8
3	1.6	1.6	1.7

Fields, Russell, Sachs, Wattenberg (Photoneutron source)

σ_t (barns)

Energy (Mev) \rightarrow	.024	.13	.14	.22	.62	.83
Be	5	4.3	4.3	4.2	3.3	3.1
B	5.5	4.9	4.7	4.3		2.3
C	4.6	4.3	4.3	4.1	3.3	2.9
O	3.6	3.5	4.1	3.0	3.5	4.9
F	3.5	5.7		6.9	4.6	4.1
Na	5.1	3.9	4.2	3.8	5.9	4.6
Mg	4.4	4.9	5.7	8.7	4.2	3.4
Al	.8	5.3	3.2	3.2	4.1	3.5
P	3.8	3.1	3.1	3.2	3.1	3.5
S	1.0	4.2	4.5	2.9		2.2
K	1.2	1.6	1.9	1.7	2.3	2.7

cont'd

Fields, Russell, Sachs, Wattenberg (cont'd)

Energy (Mev) →	.024	.13	.14	.22	.62	.83
Fe	2.2	4.1	3.9	3.3		2.7
Ni	2.3	6.4	4.2	5.8	3.7	3.5
Cu	8	6.2	5.9	5.3		3.8
Zn	9.9	6.6	5.4	5.1	4.7	4.3
Ag	8	8.1	8.1	7.8	7.3	7.2
Cd	6.9	7.6	7.3	7.3		7.1
Sn	5.9	6.4	6.4	6.3	6.8	6.7
Sb	6.3	6.9	6.4	6.1	5.7	6.4
I	7.0	6.6	6.5	6.1	6.8	6.7
W	13.8	10.	9.4	8.0	7.8	7.7
Pb	11.4	10.6	10.6	8.6	6.1	5.8
Bi	12.1	10.2	9.7	8.0		5.9

D H. Frisch

(Li + p neutrons)

σ_t (barns) on Carbon

Neutron Energy	σ_t
.35 Mev	4.63
.95	4.65
.265	3.85
.490	3.26

Good, Scharff-Goldhaber

(Ra-Th + Be neutrons)
Neutron Energy 0.9 Mev
 σ_t (barns)

Be	2.82 b
C	2.66
Al	3.39
Cu	2.78
Pb	6.83
U	8.00

Kikuchi and Aoki *

(D + D neutrons)

Neutron energy 2.46 Mev

σ_t (barns)

B	1.65
C	1.5
N	1.56
O	1.41
F	2.3
Na	3.33
Mg	1.89
Al	3.15
Si	2.95

cont'd

* The paper containing this data was unavailable. The results here are quoted from an article by C. G. Goodman to appear in Nucleonics.

Kikuchi and Aoki (cont'd)

P	3.24
S	2.38
Cl	2.78
K	4.15
Ca	3.85
Ti	1.73
Cr	3.38
Mn	3.02
Fe	3.20
Co	2.59
Ni	2.66
Cu	2.59
Zn	2.68
As	3.39
Br	2.69
Sr	4.14
Ag	4.30
Cd	4.07
Sn	3.82
Sb	4.81
I	5.40
Ba	6.19
W	6.21
Hg	5.13
Pb	5.25
Bi	6.30

McPhail

(D + D neutrons)

Energy (Mev) →	2.80	2.65	2.57	2.49	2.41	2.31
Al	2.48	2.94	2.94	2.18	2.19	2.49
Mg	2.34	2.54	2.14	1.76	1.94	2.19
C	1.57	1.45	1.38	1.38	1.39	1.41
Na	2.38	2.50	2.69	2.69	2.69	2.74
N	1.25	1.28	1.39	1.27	1.22	1.33

Nuckolls, Bailey, Bennett, Bergstrahl, Richards and Williams

(Li + p, C¹² + D, D + D neutrons)

σ_t (barns) on oxygen

Neutron Energy	σ_t
.35 Mev	4.80
.46	3.61
.72	2.01
.97	5.06
1.0 ± .1	3.86
1.6	1.43
2.0	.89
2.6	1.09
3.0	.96
3.5	2.39
4.0	2.90
4.5	1.83

cont'd

Nuckolls, Bailey, Bennett, Bergstrahl, Richards and Williams (cont'd)

Neutron Energy	σ_t
5.0	1.66
5.5	.96
6.0	1.04

R. Sherr

Neutron Energy 25 Mev

(Li + D neutrons)

Element	σ_t (barns)
C	1.29
O	1.6
Al	1.85
Cl	1.88
Cu	2.50
Ag	3.70
Hg	5.25

Zimm, Seeley and Cohen

(D + D neutrons)

σ_t (barns)

Energy (Mev) →	2.85	2.46
B	1.98	
C	1.97	1.37
N	1.38	1.40

cont'd

Zinn, Seeley and Cohen (cont'd)

Energy (Mev) →	2.85	2.46
O	1.25	1.05
Na	2.37	2.70
Mg	2.25	
Al	2.34	2.99
Si	2.77	
S	3.12	2.77
Cl	3.42	
K	3.13	3.44
Mn	3.82	
Fe	3.15	
Cu	2.82	
Zn	3.28	
Se	4.05	
Mo	4.06	
Sn	4.39	
Hg	5.34	
Pb	6.74	

A. Wattenberg
(Photoneutron Source)
 σ_t (barns) on carbon

Neutron Energy	σ_t
.024 Mev	4.55
.13	4.3
.13	4.3
.14	4.3
.22	4.1
.62	3.4
.83	2.9

Table 6

References for Inelastic Scattering

ABCT	Amaldi, Bocciarelli, Caciapuoto, Trabacchi	Nuovo Cimento <u>3</u> , 203, 1946.
AH	Allen and Hurst	Proc. Phys. Soc. London, <u>52</u> , 501, 1940.
BBBGJM	Barschall, Battat, Bright, Graves, Jorgensen, and Manley	Phys. Rev. <u>72</u> , 881, 1947
CG	Collie and Griffiths	Proc. Roy. Soc. London <u>155a</u> , 434 (1936)
F	Feld, B. T.	Phys. Rev. <u>75</u> , 1115, 1949.
FSS	Feld, Scalettar, and Szilard	Phys. Rev. <u>71</u> , 464A, 1947.
GEB	Gittings, Everhart and Barschall	Phys. Rev. <u>75</u> , 1610L, 1949.
GrS	Graham and Seaborg	Phys. Rev. <u>53</u> , 795, 1938.
PD	Phillips and Davis	Unpublished.
Sa	Sagane	Phys. Rev. <u>53</u> , 492, 1938.
SR	Salant and Ramsey	Phys. Rev. <u>57</u> , 1075A, 1940.
So	Soltan	Nature, 1938.

C. Inelastic Scattering Cross-sections (For table of references see Table 6)

The neutrons emitted in inelastic scattering processes have been observed by means of two types of threshold detectors (1) radioactive and (2) recoil. In the radioactive threshold detectors neutron reactions, which require at least a minimum neutron energy, called the threshold energy E_t , are utilized to detect neutrons with energies greater than E_t . Recoil detectors employ the effects of the recoil particles, usually protons. In the experiments of BBBGJM the ionization of the recoil protons was measured; the instrument was biased so that recoils with at least a certain energy were measured. In recent work by a Los Alamos group (to be published in Rev. Sci. Inst.) photographic plates are used as detectors of the recoil particles. The radioactive detectors have the advantage of operational ease, but the disadvantage of a very gradual approach of the sensitivity to maximum value, and its irregular behavior once the maximum sensitivity is achieved. The ionization recoil detector has the advantage of flexibility with regard to energy threshold, and a better determination of E_t . The disadvantages lie mostly in the low intensity resulting from the necessary collimation, and some uncertainty in the value of E_t . The photographic film recoil detector overcomes most of these disadvantages and should prove very useful in the energy range above say 5 Mev. Below this the ionization recoil detector will probably be most useful.

The various radioactive threshold detectors employed in the measurement of inelastic scattering together with a nominal threshold energy and the radioactive half life are given in Table 7 below. Immediately below this, in Table 8, we quote the theoretical results of FSS on the energy sensitivity of some of the detectors. As mentioned earlier there is a gradual approach of radioactive detectors to their full sensitivity as the neutron energy is increased. The nominal threshold employed in Table 7 is placed approximately at the energy at which the yield is 50% of the maximum.

Table 7

Detector	Reaction	Half Life	Nominal Threshold	Reference
C ¹²	C ¹² (n,2n)C ¹¹	20.5 m	20.4 Mev	S
Al ²⁷	Al ²⁷ (n,p)Mg ²⁷	10.2 m	4.5	FSS
Al ²⁷	Al ²⁷ (n,α)Na ²⁴	14.8 h	9.	FSS
Si ²⁸	Si ²⁸ (n,p)Al ²⁸	2.4 m	5.	FSS
P ³¹	P ³¹ (n,p)Si ³¹	170.0 m	4.	FSS
P ³¹	P ³¹ (n,α)Al ²⁸	2.4 m	8.5	FSS
S ³²	S ³² (n,p)P ³²	14.3 d	4.	FSS, GrS
Fe ⁵⁶	Fe ⁵⁶ (n,p)Mn ⁵⁶	2.6 h	7.	Sa
Cu ⁶³	Cu ⁶³ (n,2n)Cu ⁶²	10.5 m	12.	SR
Ag ¹⁰⁷	Ag ¹⁰⁷ (n,2n)Ag ¹⁰⁶	24.5 m	5.	Sa, GrS

Table 8

Detector	Threshold	Energy for which yield is 10% of maximum	Energy for which yield is 50% of maximum
Al ²⁷ (n,p)Mg ²⁷	1.95 Mev	3.6 Mev	4.6 Mev
Al ²⁷ (n,α)Na ²⁴	2.39	7.5	9.1
Si ²⁸ (n,p)Al ²⁸	2.69	4.5	5.5
P ³¹ (n,p)Si ³¹	1.02	2.9	3.9
P ³¹ (n,α)Al ²⁸	.90	6.6	8.3

Table 9

Inelastic Cross-sections Obtained with Radioactive Threshold Detectors

Neutron Energy 14 Mev (detector Cu(n,2n))

Element	Observed σ	Theory	Reference
Al	.90 b	.93 b	AECT
	1.06		PD
	1.25		So
Fe	1.45	1.3	ABCT
	1.43		PD
	1.25		So
Cu	1.5	1.25	So
Ag	1.7	1.8	So
Cd	1.89	1.9	PD
Sn	1.8	2.0	So
Au	2.51	2.2	PD
Hg	2.47	2.5	ABCT
Bi	2.56	2.3	PD
	2.7		So
Pb	2.22	2.3	ABCT
	2.29		GEB
	2.56		PD
	2.7		So

Table 10

(Ra-Be neutrons) (Detector, Fe⁵⁶(n,p)Mn⁵⁶)

Element	Observed σ	Theory	Reference
Al	.93 \pm .13b	.9 b	GrS
Zn	1.54 \pm .15	1.33	GrS
Sb	1.79 \pm .23	1.93	GrS
Bi	2.32 \pm .20	2.2	GrS
Pb	2.13 \pm .24	2.1	GrS

The experimental values for the total inelastic cross-section are given in Table 9 together with the theoretical predictions. In Table 10 measurements of Graham and Seaborg utilizing a (Ra-Be) source are given together with theoretical predictions. The theoretical values given in these two tables (9 and 10) are computed on the assumption that inelastic and other absorption processes are dominant for the energies involved. In the Graham-Seaborg data we have employed average values for σ_c above 7 Mev which are in error by at most 10%. The comparison with theory and experiment is excellent. On the whole the experimental values obtained by So seem high relative to those of ABCT, GIEB and GrS. We suspect that only the first figure of Soltan's data is significant.

Some of the elements listed in Table 9 have been measured with other radioactive threshold detectors of lower E_t . In principle, this would yield some information with regard to the energy distribution of the emerging neutrons. Similar data are available for Table 10 but because of the broad energy spread of the incident neutrons it is very difficult to obtain equivalent information. Unfortunately the data are poor so that not much can be said. Qualitatively, however, one may safely say that it is probable for high energy neutrons to lose a great deal of their energy upon their first inelastic collision so that the energy distribution of the emerging neutrons has a maximum in the low energy region. The results obtained by So, GrS, GEB have been tabulated in Tables 11 and 12 below for the sake of completeness.

Experiments employing $P^{31}(n,p)Si^{31}$ detector and D-D neutrons at 3.25 Mev have been performed by Allen and Hurst. Examination of Table 7 giving the characteristics of this detector reveals that these authors were working in an energy region for which the detector was relatively insensitive, thus making it probable that serious background difficulties developed. The values given

Table 11

Inelastic Cross-sections with Radioactive Threshold Detectors with
Relatively Small E_t . Neutron Energy 14 Mev

Detector a) $Al^{27}(n,p)Mg^{27}$
b) $Ag^{107}(n,2n)Ag^{106}$

Element	Detector a	Detector b	Reference
Al	1 barn	1.1 barn	So
Fe	1.6	1.6	So
Cu	1.8	1.7	So
Zn	1.8	1.6	So
Ag	2.1	2.2	So
Sn	1.8	2.0	So
Pb	2.2		GEB
	2.7	2.7	So
Bi	2.5	2.5	So

Table 12

Inelastic Cross-sections with Radioactive Threshold Detectors with
Relatively Small E_t . Neutron Energy 14 Mev

Ra-Be neutron source.

Detector a) $Al^{27}(n,p)Mg^{27}$
b) $Si^{28}(n,p)Al^{28}$

Element	Detector a	Detector b	Reference
C	.42 barns		GrS
Al	.78		GrS
Cu	1.3		CG
Zn	1.59		CG
Cd	1.5	1.0 barns	CG
Sn	1.71		GrS
		1.4	CG

cont'd

Table 12 (cont'd)

Element	Detector a	Detector b	Reference
Sb	1.76		GrS
Pb	1.97	1.4	GrS
	1.8		CG
Bi	1.98	1.3	GrS
			CG

by Allen and Hurst are much too large. They are considerably larger than (1) those obtained by BBBGJM at approximately the same energy, (2) the inelastic cross-sections obtained at higher energies and (3) the cross-sections expected theoretically.

Hydrogen filled recoil threshold detectors have been employed by Barschall et al (BBBGJM) to determine inelastic scattering cross-sections and the energy distribution of the emitted neutrons for incident neutrons, 1.5 Mev (Li + p source) and 3.0 Mev (D+D source). These experiments required corrections for multiple scattering. These corrections have been applied to Fe, W, Pb only. In the tables below we list all elements measured together with these for Fe, W, Pb, for which we list both the corrected and uncorrected value so that some idea as to the order of magnitude of the correction may be obtained. The former is underlined. The value of E_c corresponding to each bias voltage was taken from Feld. The elements Fe, W, Pb will be discussed in detail later in this report. The main conclusions are: (1) W and Pb obey the statistical theory; in W practically from zero excitation energy; in Pb from above 1 Mev; (2) experimental results for Fe do not agree with theoretical results employing the level scheme for Fe⁵⁶ obtained from the radioactive decay of Mn⁵⁶; (3) the magnitude of the cross-sections is considerably larger than theory predicts. This discrepancy

Table 13

Cross-sections for the Inelastic Scattering of 1.5 Mev neutrons to
Energies Less than the Threshold Energies *

Element	Threshold Energies		
	.40 Mev	.90 Mev	1.30 Mev
Fe	0 barns	<u>.6</u> barns <u>.7</u>	
Ni	0	.1	.6 barns
Co	0	.2	.8
Cu	.3	.6	.9
Ta	1.4	2.0	2.7
W	<u>.9</u> <u>.6</u>	<u>2.1</u> <u>1.6</u>	
Pb	0	<u>.4</u> <u>.4</u>	

* All values quoted have not been corrected except those underlined.

3.0 Mev neutrons incident

Element	Threshold Energies		
	.95 Mev	1.5 Mev	2.25 Mev
Fe	<u>.3</u> barns <u>.5</u>	<u>.7</u> barns 1.0	<u>1.1</u> barns <u>1.4</u>
Cu	.6	1.3	1.5
Au	2.1	2.8	3.0
W	<u>1.4</u> <u>1.8</u>	<u>2.4</u> <u>2.5</u>	<u>2.8</u> <u>2.8</u>
Pb	<u>.7</u> <u>.7</u>	<u>1.2</u> <u>1.2</u>	<u>1.6</u> <u>1.6</u>

is especially marked in tungsten. In view of the rather nice agreement of theory and σ_t in this energy range, it would seem that the experimental values are suspect. Other qualitative conclusions which we may obtain from the table include (1) Ta and Au have low lying excited levels and probably conform to statistical theory and (2) the light elements Ni, Co, Cu, have but a few levels in this energy region. We may expect that Ni and Co have no excited levels below .4 Mev while Cu has one.

In summary, inelastic scattering cross-sections are available for several elements for 14 Mev and Ra-Be neutrons. Some idea as to the energy distribution of the emitted neutrons may be obtained. This will not be very accurate. However, one may make the qualitative statement that the peak in energy distribution occurs at relatively low energies. Inelastic scattering has also been observed for 3 Mev and 1.5 Mev neutrons. Multiple scattering corrections have been made for Fe, W, and Pb but not for the other few measured elements. These experiments are difficult to perform and difficult to evaluate. It would be stretching a point to put too much reliance on the final results. Since these are the only data in the Mev region, it would be extremely valuable if further experiments were performed.

D. Transport Cross-section

Transport cross-sections have been measured by BBGJM for incident neutrons with energies of .2, .6, 1.5 and 3 Mev. We tabulate below those cases for which the multiple scattering corrections have been made. Theoretical estimates based on non-resonance theory are given.

Table 14

Transport Cross-sections

Neutron Energy Element	.2 Mev		.6 Mev		1.5 Mev		3 Mev	
	obs.	theo.	obs.	theo.	obs.	theo.	obs.	theo.
Be			3.4b	1.8b	1.4b	1.4b		
B ¹⁰			3.9		2.1			
B ¹¹			2.1	2.0	2.2	1.5		
C			2.8	2.1	1.8	1.6		
Al			3.0	2.4	1.7	1.8	1.4b	1.5b
Fe	3b	3.4b	2.0	2.4	2.2	1.8	2.0	1.5
Pb	7	6.1	3.4	4.5	3.4	3.7	3.8	3.2
W	6	6.4	4.7	4.7	4.7	3.8	4.1	3.4
Au	6.4	5.9						

Agreement with the non-resonance theory is relatively good considering that in this energy region it holds only on the average.

These are the only measurements made of transport cross-sections although some of the experiments performed by the Japanese may be evaluated to obtain σ_{tr} . These, however, have not been corrected for inelastic scattering.

E. Particular Elements

1. Boron

The most recent measurements on neutron transmission through boron have been made by Barschall, Battat and Bright (Phys. Rev. 70, 458, 1946) and Fields, Russell, Sachs, Wattenberg (Phys. Rev. 71, 508, 1947). The former used a Li(p,n) source and measured the cross-sections up to 1.5 Mev for both natural and enriched boron, so that σ_t for both B¹⁰ (abundance, .184) and B¹¹ (abundance, .816) are

known. They also obtained one point at 3 Mev with a D-D source. We have plotted these results in Figs. 20 and 21. FRSW employ photoneutron sources. Unfortunately their data disagree with BBB. For example, at .8 Mev BBB obtain $\sigma_t = 1.8$ b, while FRSW obtain $\sigma_t = 2.3$ b at .83 Mev. Pre-war measurements have been made by Aoki (Proc. Phys. Math. Soc. of Japan, 21, 232, 1939) by Kikuchi and Aoki (Proc. Phys. Math. Soc. of Japan, 21, 75, 1939) and Zinn, Seeley and Cohen (Phys. Rev. 56, 260, 1939) with neutrons from the D-D reaction. Aoki data are given earlier in this report. Kikuchi and Aoki obtain $\sigma_t = 1.65$ b at $E = 2.5$ Mev; Zinn, Seeley and Cohen obtain 1.98 b at 2.88 Mev, while Aoki finds 2.4 b at 2.5 Mev and 2 b at 2.8 Mev. It is clear that the data are not consistent. The differences may be in part caused by voltage calibration errors. They may also indicate resonances in the 1.5 - 3 Mev region which would have been missed by BBB. A resonance at 1.85 Mev is indicated by their data and also shows up in the cross-section for the (n- α) reaction on B^{10} as obtained by Bailey et al quoted by Goldsmith, Ibser and Feld. It is clear that more measurements in the fast neutron energy region are needed.

We have compared the experimental data with the predictions of the non-resonance theory with the experiment of ABCT who give $\sigma_t = 1.16$ b at $E = 14$ Mev. The comparison indicates that this is the proper radius in this energy range as well and permits the extrapolation indicated in the figures. The theory has also been compared with the measured (n, α) cross-section for B^{10} . The effect of the Coulomb field on the α particle was neglected and the widths involved were computed via equations (28a) and (27a) of the text (with, of course, the necessary changes for the mass of the α particle). The agreement is excellent permitting the extrapolation of this cross-section as well

as the prediction of the inelastic cross-section for both B^{10} and B^{11} , and the (n,α) reaction on B^{11} which has a threshold at 6.66 Mev. (Hornyak and Lauritsen, Rev. Mod. Phys., 20, 191, 1948). Lauritsen (Prel. Rep. No. 5, Div. Math. and Phys. Sciences, NRC) has tabulated the known levels in B^{10} and B^{11} permitting the estimate of \bar{D} , the average level separation. For B^{10} , $\bar{D} = .7$ Mev, $E_0 = .411$ Mev while for B^{11} , $\bar{D} = 2.2$ Mev and $E_0 = 2.1$ Mev. E_0 is the energy of the first excited level above the ground state. The figures give the results up to $E = 4.8$ Mev. The non-resonance theory predictions are given in the table below for two energies above this one.

E	\sqrt{E}	σ_t	B^{10}		B^{11}		natural B	
			σ_{in}	$\sigma(n,\alpha)$	σ_{in}	$\sigma(n,\alpha)$	σ_{in}	$\sigma(n,\alpha)$
7.0	2.64	1.33b	.27b	.32b	.25b	.07b	.25b	.12b
15.7	3.96	1.15	.38	.165	.18	.16	.22	.16

We have not given the energy distribution of the inelastically scattered neutrons. This may be obtained from (31a).

a) Transport Cross-section. The transport cross-section including absorption has been measured for B^{10} and B^{11} by the Los Alamos group (BBBGJM). The results are:

Element	Neutron Energy	
	.6 Mev	1.5 Mev
B^{10}	3.9 b	2.1 b
B^{11}	2.1	2.2

2. Iron

a) Total Cross-section (See Fig. 16). The recent measurements of EBS are in excellent agreement with those of FRSW. Barschall's experiments below 500 k.e.v.

employed neutrons whose energy spread was 20 k.e.v. permitting the discovery of the resonances and close level spacing (60 k.e.v.) in that energy region. The width of the resonance at 30 k.e.v. is mostly due to the spread in energy of the incident neutrons; the corrected maximum cross-section is estimated to be 65 b. Above 500 k.e.v., Barschall et al utilized neutrons with an energy spread of 100 k.e.v., thus smoothing out the dependence of the cross-section on energy. It is expected that the resonances exhibited below 500 k.e.v. continue above that energy. The non-resonance region is estimated to start at about 4 to 5 Mev. The data below 1.4 Mev are consistent with the average as predicted by the non-resonance theory if a radius of 4.6×10^{-13} cm is employed. The data between 2 and 3 Mev, taken with D-D neutrons, fall somewhat above the theoretical curve. The only other datum is given by Amaldi et al who measure $\sigma_{\text{tot}} = 2.75$ b for neutrons of 14 Mev energy. This requires a radius of 5.6×10^{-13} cm. This energy dependence of the nuclear radius is not inconsistent with theoretical expectations. Note that the values obtained by Aoki at 2 - 3 Mev and by Amaldi et al are the same, so that it would be consistent with the data to assume a constant cross-section of 2.75 b for Fe for neutron energies from 2 Mev to 14 Mev.

b) Transport Cross-section (See Fig. 17). The experimental results which have been obtained by the Los Alamos group are plotted in Fig. 17 where they are compared with the average computed from non-resonance theory utilizing the radius of 4.6×10^{-13} cm determined by the experimental values of σ_t . The theory and experiment are in substantial agreement. Actually one would expect the σ_{tr} dependence to roughly parallel that of σ_{tot} so that more precise measurements would show many resonances. The rather large deviation from the average curve at 3 Mev may be caused by a resonance; however, if Aoki's results are taken at face value, the deviation is probably experimental error. Note that the theoretical transport cross-section even at 9 Mev, $\sigma_{\text{tr}}/(\pi R^2) = 1.9$, is still very much larger than the asymptotic value of 1.

c) Inelastic Cross-section. The inelastic cross-section at 14 Mev has been measured by Amaldi et al, and by Phillips and Davis at Los Alamos. They obtain 1.43 b and 1.45 b respectively. The theory assuming $\sigma_{in} \approx \sigma_c$ and $R = 5.6 \times 10^{-13}$ cm gives $\sigma_{in} = 1.3$ b.

Measurements have also been made by the Los Alamos group at 3 Mev and 1.5 Mev and are presented in the table below:

Incident Neutron Energy	Threshold Energy	Cross-section for Inelastic Scattering of Neutrons to Energies Less Than the Threshold Energy	Energies of the Emitted Neutrons
1.5 Mev	.40 Mev	0 b	---
	.90	.6	.55 Mev
3.0	.75	.3	.4
	1.50	.7	.9, .4
	2.25	1.0	2.15, .9, .4

Feld has pointed out (Phys. Rev. 75, 1115, 1949) the qualitative behavior of these results may be understood in terms of excited levels of Fe at .85, 2.1, 2.6 Mev, which have been observed by Deutsch et al. The consequent energies of the neutron groups included in each measurement are given in the fourth column of the table. If these are assumed to be the only excited levels of Fe, one must conclude that the emission of each of the three possible groups occurs with about equal probability. This is not in agreement with estimates based on the average results discussed in Section II of this report. There it is estimated that the relative weight of each neutron group is proportional to its energy. The total

inelastic cross-section of 1.1 b at 3 Mev is large, for the predicted σ_c is 1.06 b, and one may expect appreciable incoherent scattering at these energies. This deviation is precisely the one noted for σ_{tr} above. A similar situation prevails at 1.5 Mev; the theoretical σ_c is found to be 1.26 b. To obtain the experimental results at this energy it would be necessary to assume equal probability for the emission of neutrons of 1.5 Mev and of .55 Mev.

3. Tungsten

- a) Total Cross-section (See Fig. 18). Barschall et al have measured the total cross-section of W for neutrons up to neutron energies of 1.4 Mev. FRSW have made measurements at energies below 1 Mev. In the D-D neutron energy range, we have the measurements of Aoki, and Kikuchi and Aoki. The experimental data agree very well with the theoretical curve computed from non-resonance theory when a radius $R = 7.8 \times 10^{-13}$ is employed. There are not any strong resonances present; indeed on a statistical model, the non-resonance behavior is expected to be dominant at an energy somewhat greater than .3 Mev.
- b) Transport Cross-section (See Fig. 19). The experimental values obtained by the Los Alamos group agree fairly well with the non-resonance theory curve employing $R = 7.8 \times 10^{-13}$ cm. The experimental values do exceed the predicted values at three of the four energies and by a particularly large amount at 1.5 Mev. This last deviation must be considered excessive inasmuch as there do not seem to be any resonances present in this energy region.
- c) Inelastic Scattering. The only measurements of inelastic scattering of tungsten are those performed by the Los Alamos group quoted below:

(over)

Incident Neutron Energy	Threshold Energy	Cross-section for Inelastic Scattering of Neutrons to Energies Less Than Threshold Energy
1.5 Mev	.40 Mev	.9 b
	.90	2.1
3.0	.75	1.4
	1.50	2.4
	2.25	2.8

Experimental evidence indicates that the distance between levels in tungsten is small and suggest using the statistical method. In agreement with Feld we find that

$$D \sim e^{-\sqrt{48E}}$$

Using this level distance and assuming 2.8 b for the threshold energy of 2.25 Mev, we find

Threshold Energy	σ_{exp}	$\sigma(\text{predicted})$
2.25 Mev	2.8 b	
1.5	2.4	2.58 b
.75	1.4	1.55
3.0		2.82

In the 1.5 Mev case, assume 2.1 b for threshold energy of .90 Mev with the following results:

Threshold Energy	σ_{exp}	$\sigma(\text{predicted})$
.90 Mev	2.1 b	
.40	.9	1.0 b
1.5		2.33

The predicted values of the total inelastic cross-section are not in agreement with the non-resonance theory, for employing $R = 7.8 \times 10^{-13}$ cm it yields 2.1 and 2.0 b for 3 and 1.5 Mev respectively. Again, in view of the absence of resonances in this region, the difference between experiment and theory seems excessive.

4. Lead

a) Total Cross-section (See Fig. 14). The measurements of Barschall, Bockelman, and Seagondollar, Fields, Russell, Sachs and Wattenberg, and Bretscher and Murrall (quoted in Goldsmith, Ibser and Feld) are in remarkably good agreement. Several D-D neutron measurements are given, and at 14 Mev Amaldi et al find $\sigma_t = 5.05$ b. From the non-resonance theory the cross-section at 14 Mev yields $R = 7.8 \times 10^{-13}$ cm. This value of R is used in calculating the theoretical curve in the energy region up to 3 Mev. A slightly smaller R, 7.5×10^{-13} , would yield much better agreement with theory and experiment in this energy region. We note that Barschall et al used fine resolutions below 500 k.e.v. only. Scattering resonances with the typical minima seem to be present at $E \sim .33$ Mev and $E \sim .5$ k.e.v.

b) Transport Cross-section (See Fig. 15). The transport cross-sections as measured by the Los Alamos group are in excellent agreement with theory if a radius of 7.8×10^{-13} cm is employed. If, however, the somewhat smaller radius indicated by σ_t behavior (see above) is used, the experimental points would be found to be systematically above the theoretical curve.

c) Inelastic Scattering. At 14 Mev, Amaldi et al report $\sigma_{in} = 2.22$ b, Gittings, Barschall, and Everhart report $\sigma_{in} = 2.29$ b, while Phillips and Davis obtain 2.56 b. Theory with $R = 7.8 \times 10^{-13}$ required to match 14 Mev σ_{tot} of Amaldi yields 2.2 b. Gittings et al employed an Al(n,p) detector as well as the Cu(n,2n). These have nominal thresholds at 4.5 and 11 Mev respectively. With Al detector, they obtain 2.22 b, a rather small change. Assuming statistical theory this yields some information about " α " in the formula for level density. We find that $\alpha \simeq 20(\text{Mev})^{-1}$ if the

aluminum threshold is taken as 4.5 Mev. If $\alpha \approx 15(\text{Mev})^{-1}$, it is necessary to raise the effective threshold to 7 Mev.

Inelastic scattering experiments have also been made at lower energies by the Los Alamos group.

Incident Neutron Energy	Threshold Energy	Cross-section for Inelastic Scattering of Neutrons to Energies Less Than the Threshold Energy
1.5 Mev	.40 Mev	0 b
	.90	.4
3.0	.75	.7
	1.50	1.2
	2.25	1.6

The results indicate that neutrons with energies between 2.25 and 1.5 Mev are somewhat less important than the neutrons with energies between 1.5 and .75 Mev, and that this latter group of neutrons is somewhat less important than the neutrons with energies between .75 and zero. This implies an increasing density of levels as expected. The following guess as to levels, etc., leads to the correct total cross-section as well as energy distribution of the emitted neutrons. Let there be no levels between 0 and .75 Mev inasmuch as Pb should behave like a light nucleus and because of some slight experimental evidence to this effect. Let there be one level between .75 and 1.5 Mev with a weight of 2 corresponding to a level at 1 Mev. Let there be 3 levels between 1.5 and 2.25 Mev corresponding to an average energy of 2 Mev and thus having a total weight of 3 and between 2.25 and 3 let there be 9 levels having an average energy of 2.6 Mev and thus a total weight of 3.6. The cross-section for the formation of the compound nucleus σ_0 is 2.19 b, so

that the predicted cross-sections for this model are 1.62 b, 1.24 b, and .63 b. The predicted cross-section at 1.5 Mev for a threshold of .9 Mev is .5 b. The level scheme is not as unreasonable as might first appear for it agrees with an average spacing $D \sim e^{-\sqrt{20E}}$ predicted from the 14 Mev experiments discussed above. It suggests that the magic number character of lead is no longer in evidence once sufficient excitation energy is available. A level scheme in which D does not decrease so rapidly is employed by Feld who assumes that only $l = 0$ neutrons participate in these reactions. However this implies a rather rigid selection rule for these relatively large values of x .

Additional Note About the Curves

The curves of total cross sections for the elements O, C, Mg, Si, S, (figures 22 to 29), were obtained from the Minnesota group under Prof. Williams, after the main body of this report had been prepared.

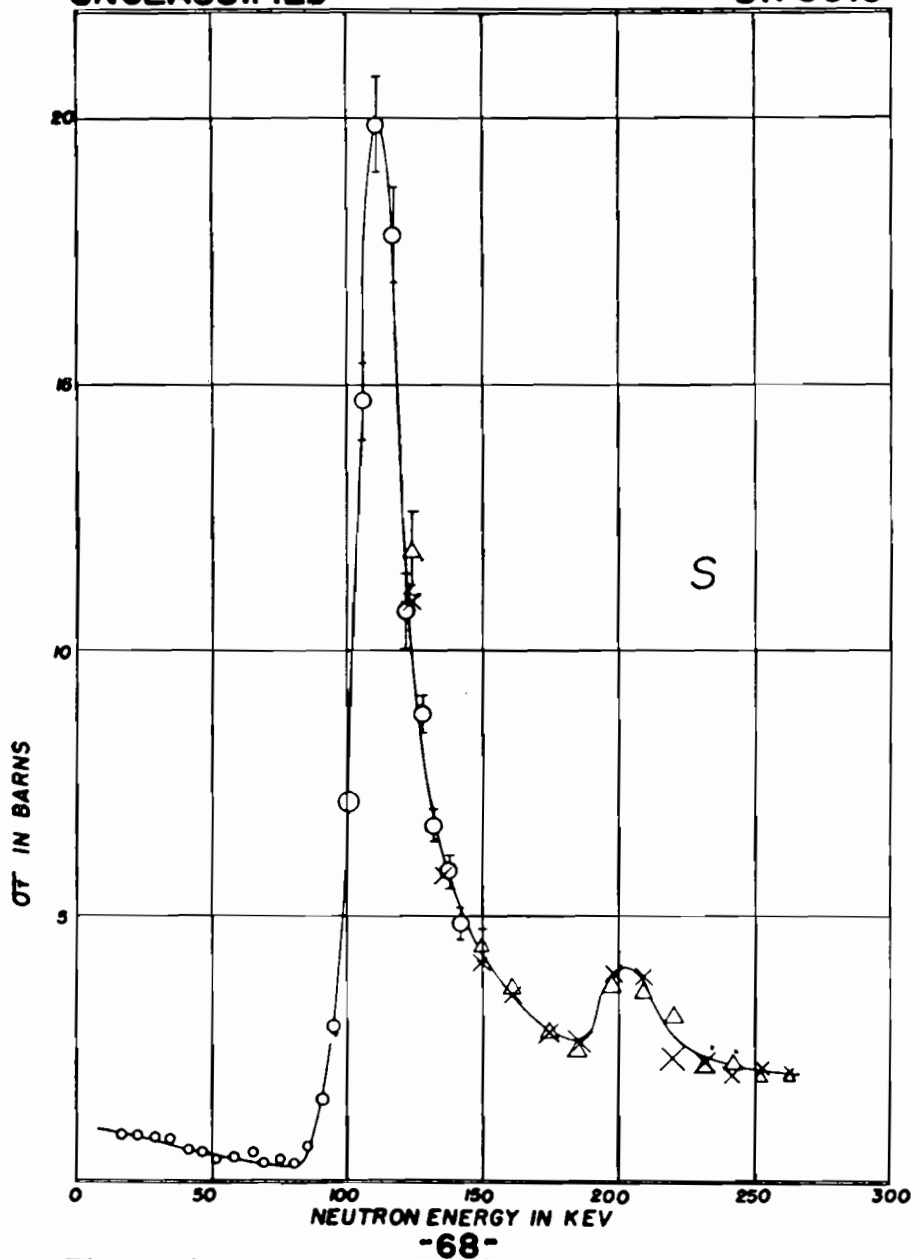


FIG. 1. The total cross section of sulfur as a function of neutron energy. The circles represent data taken at an angle of 115° with respect to the protons incident on the Li target. Other symbols show data taken in the forward direction. The height of the symbols is a measure of the statistical error.

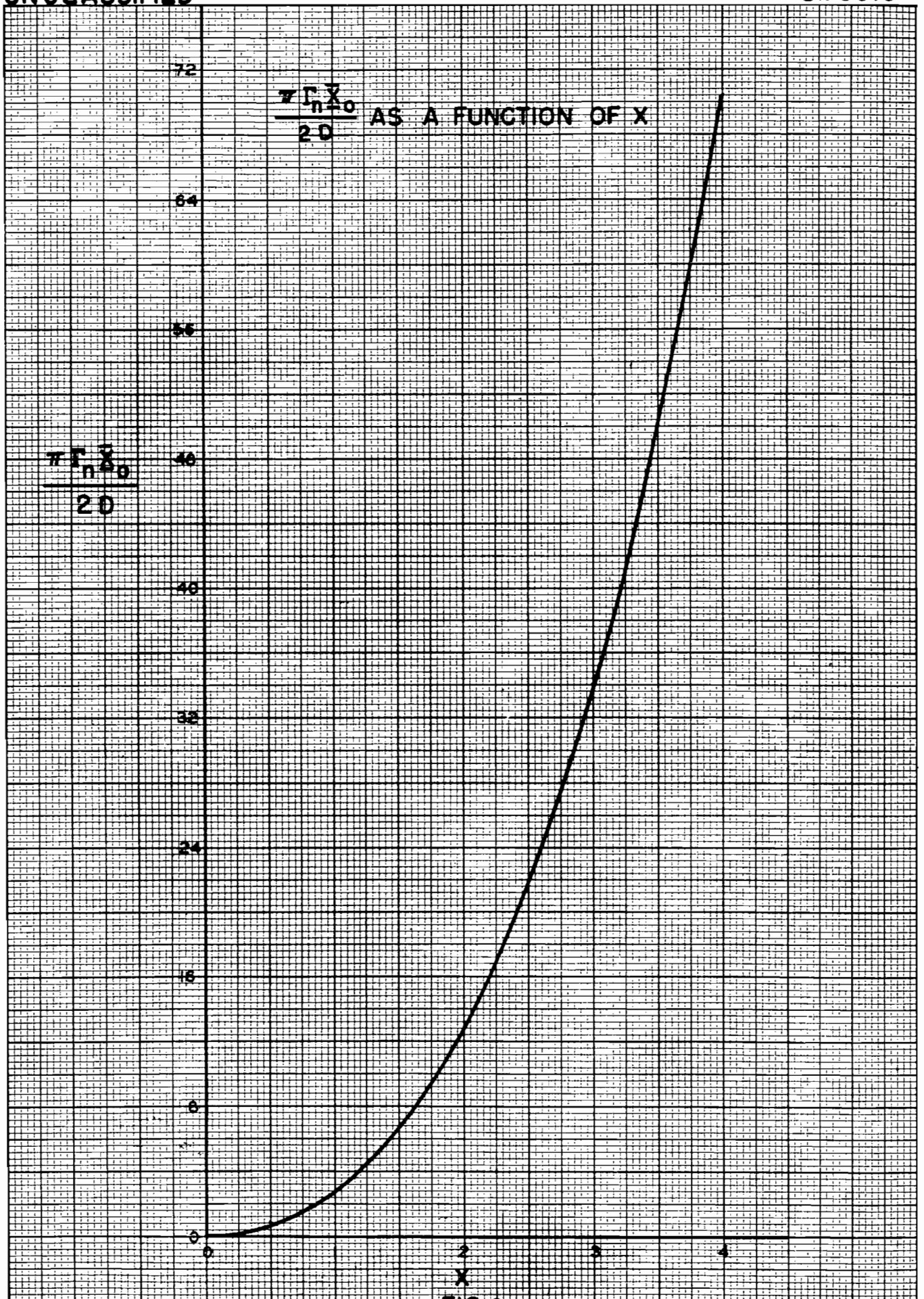
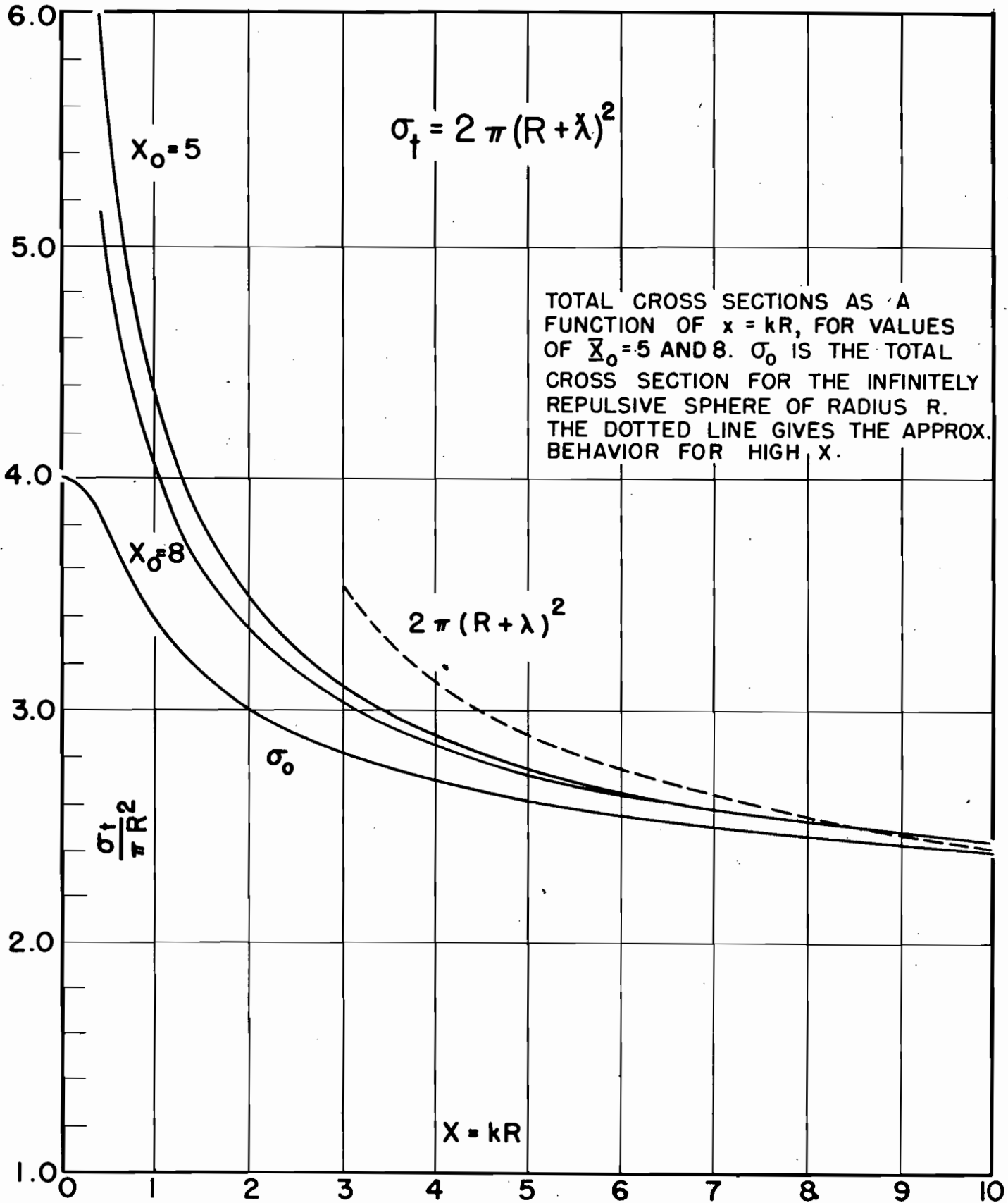


FIG. 2
-69-



TOTAL CROSS SECTIONS AS A FUNCTION OF $x = kR$, FOR VALUES OF $X_0 = 5$ AND 8. σ_0 IS THE TOTAL CROSS SECTION FOR THE INFINITELY REPULSIVE SPHERE OF RADIUS R. THE DOTTED LINE GIVES THE APPROX. BEHAVIOR FOR HIGH X.

FIG. 3
-70-

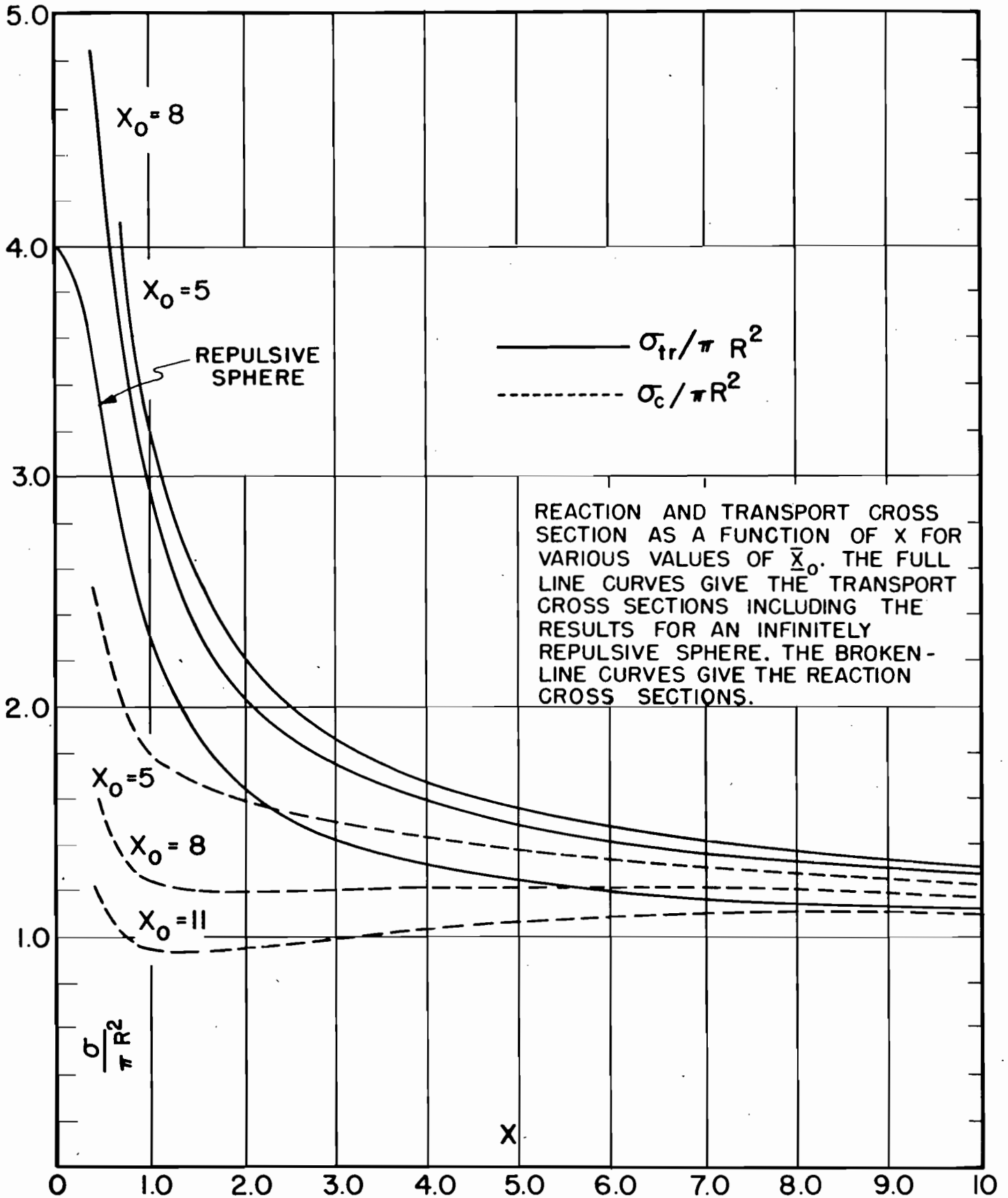
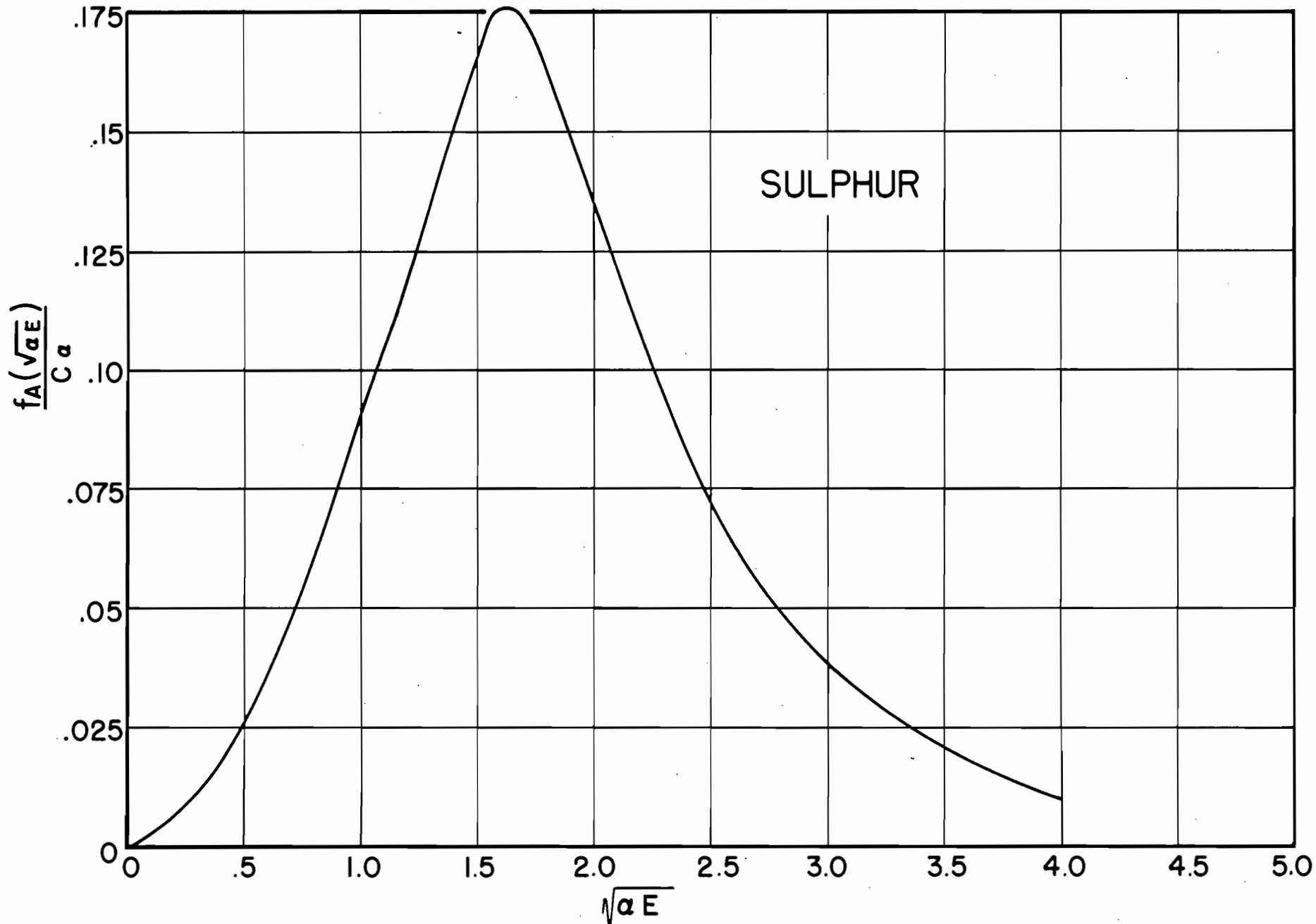


FIG. 4



SCATTERING RESONANCE OF SULPHUR

FIG. 5

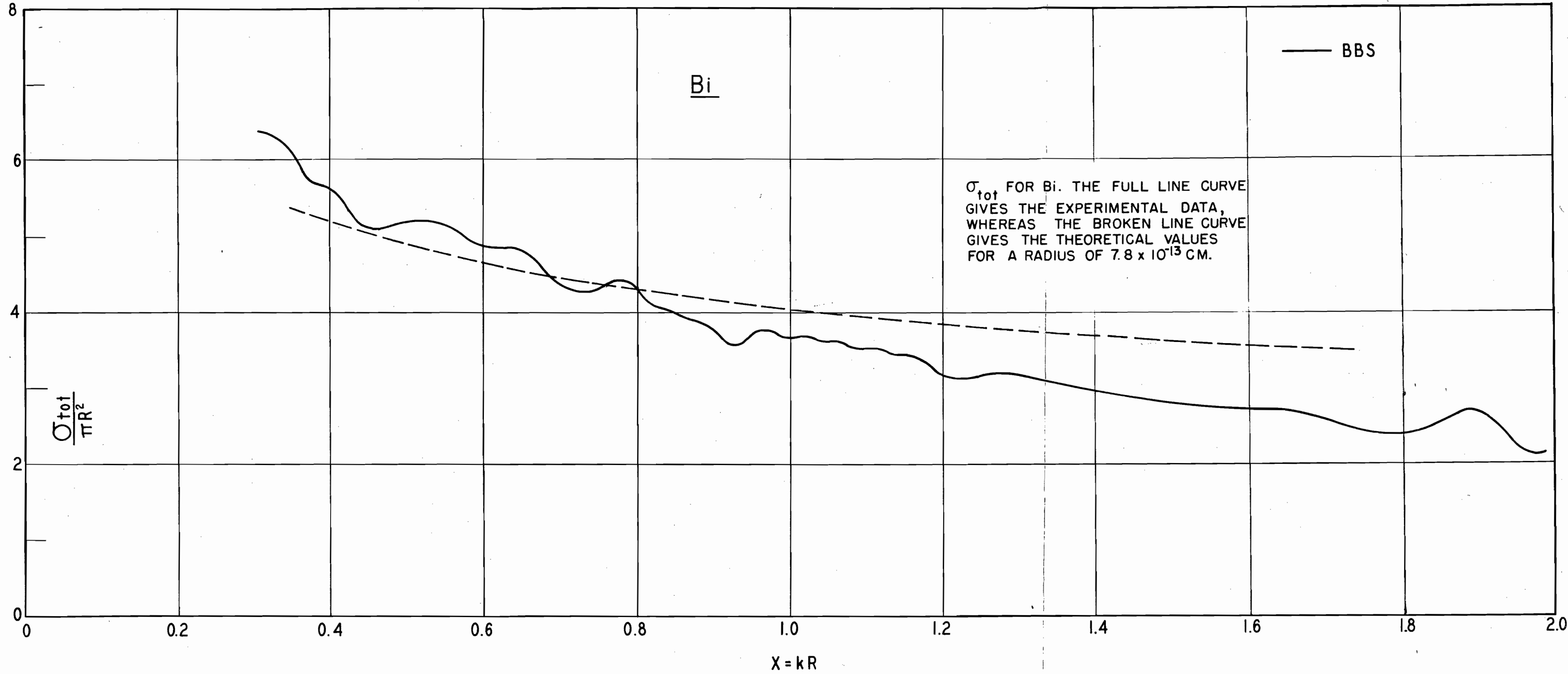
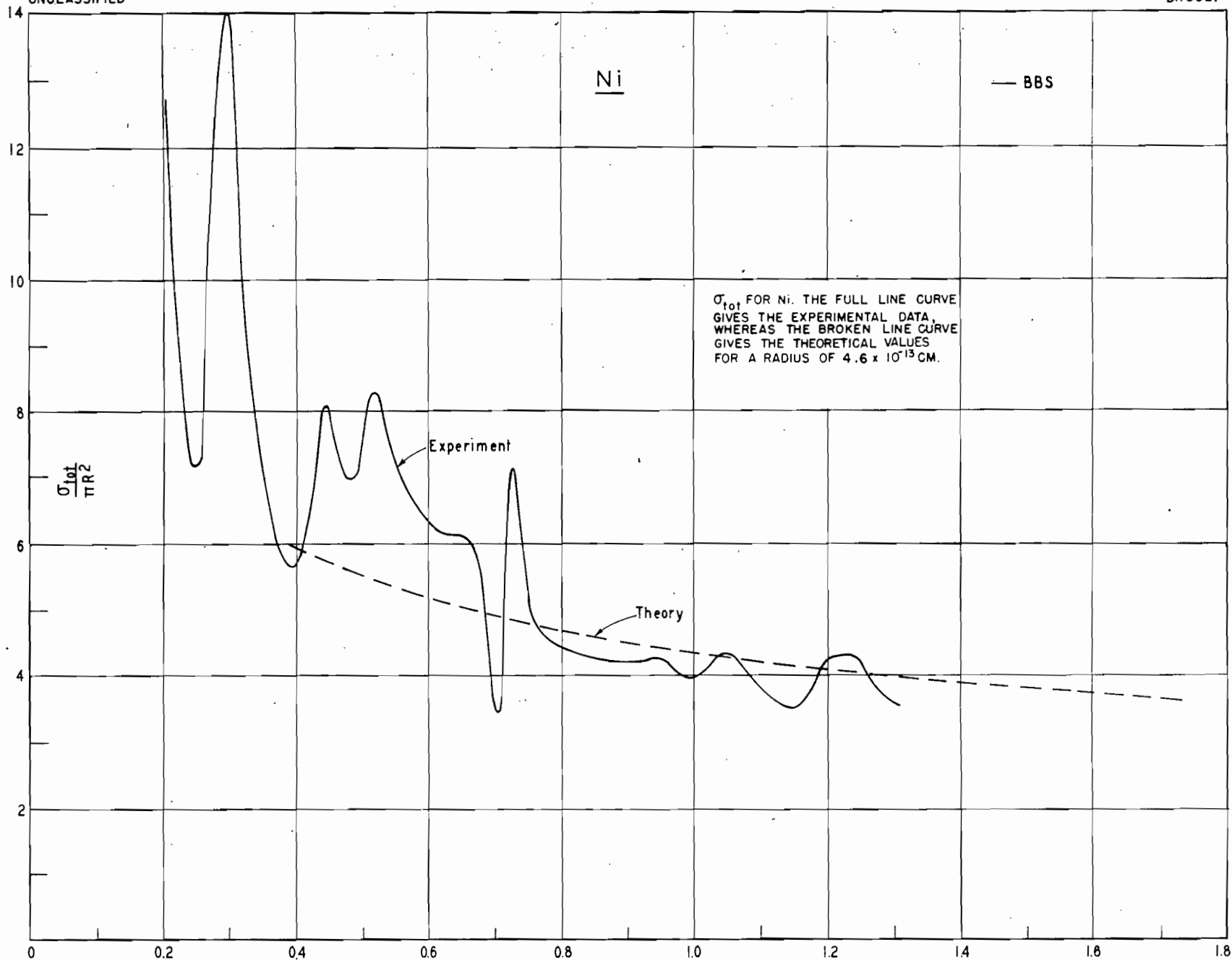


FIG. 6

X = KR
FIG. 7

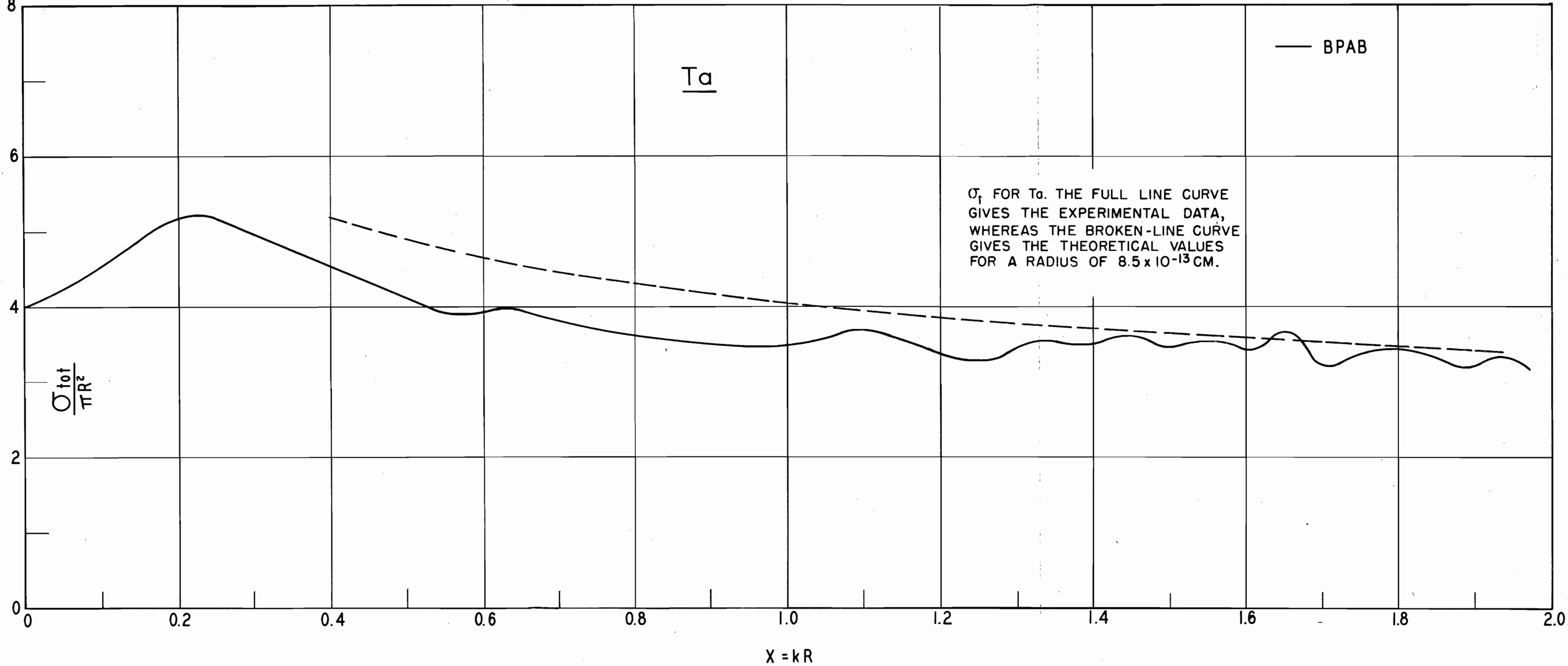
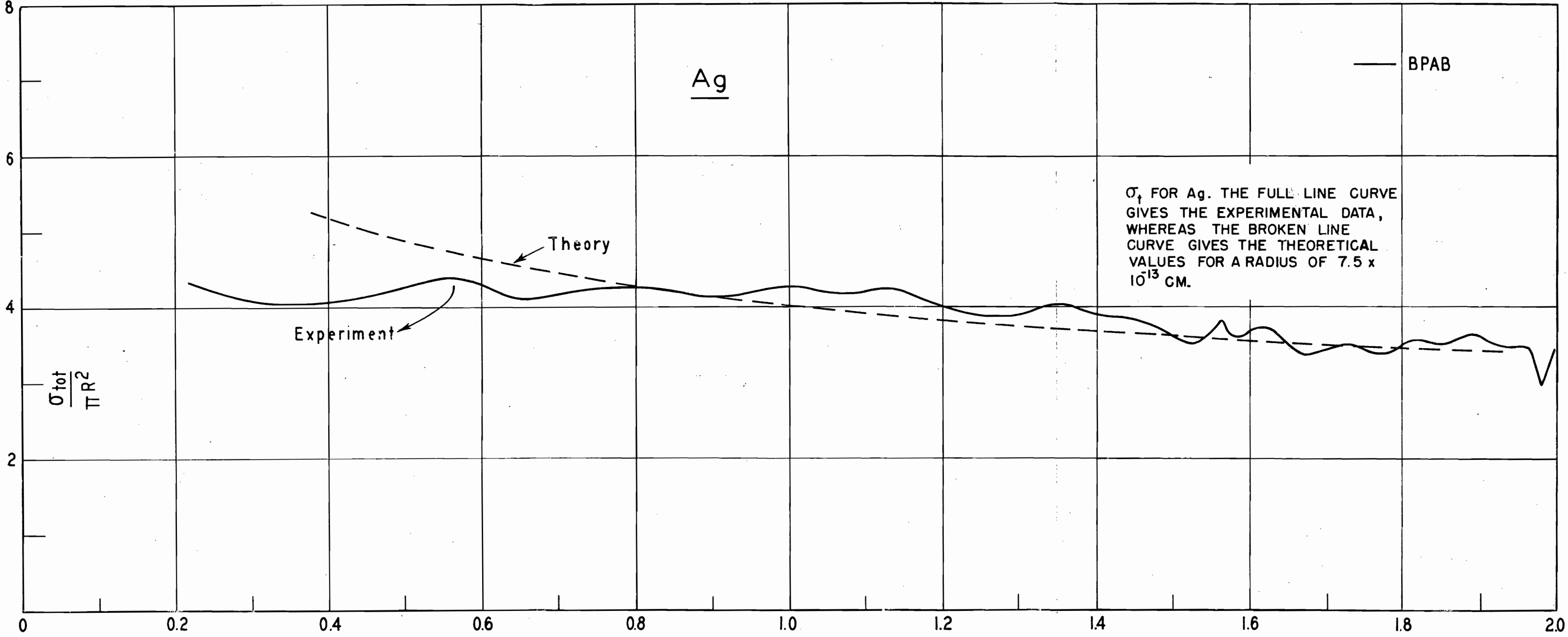


FIG. 8
-75-



X = kR
FIG. 9
-76-

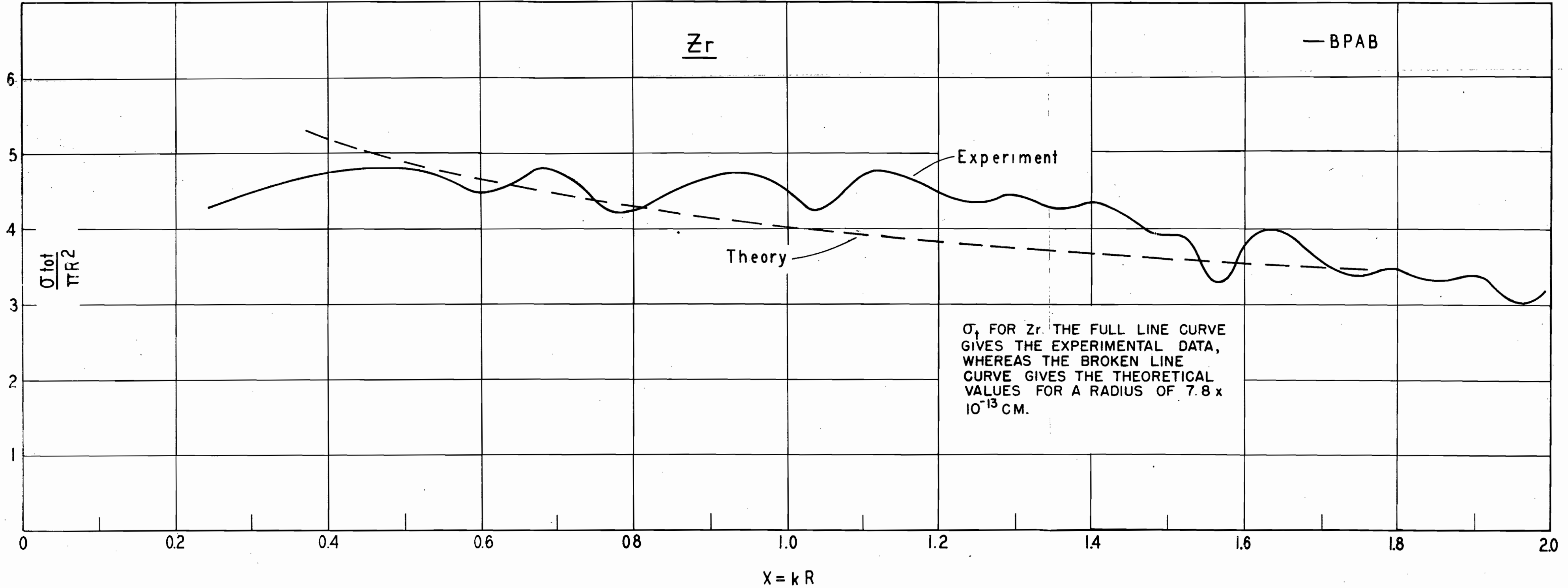
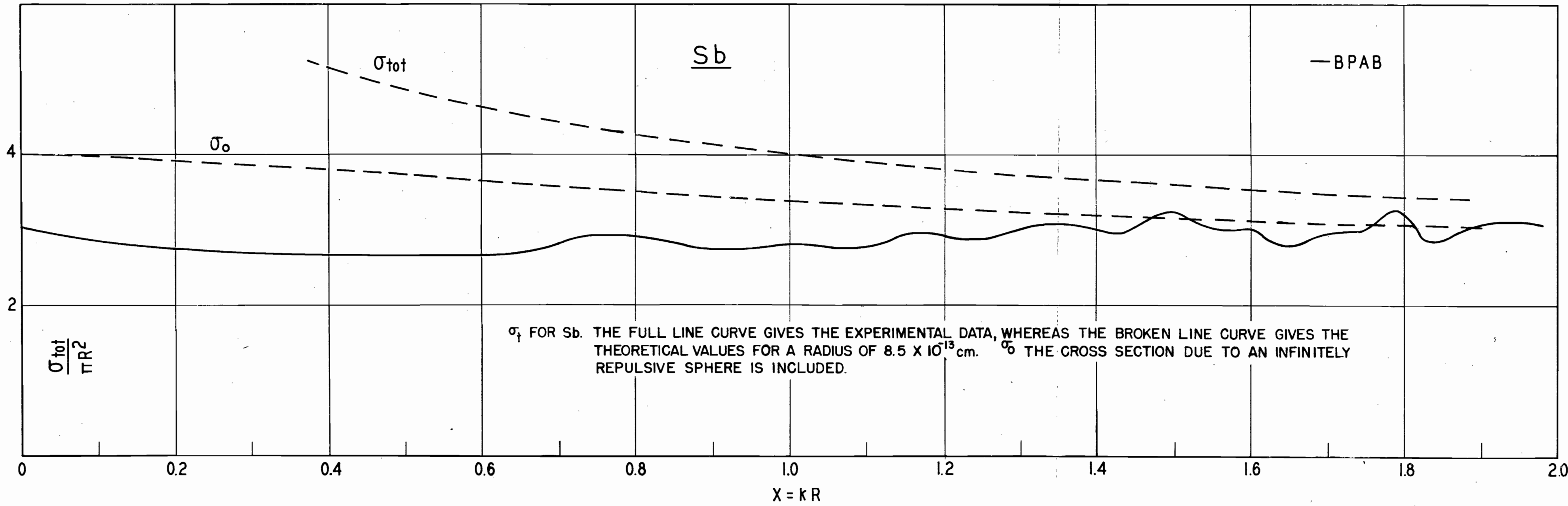
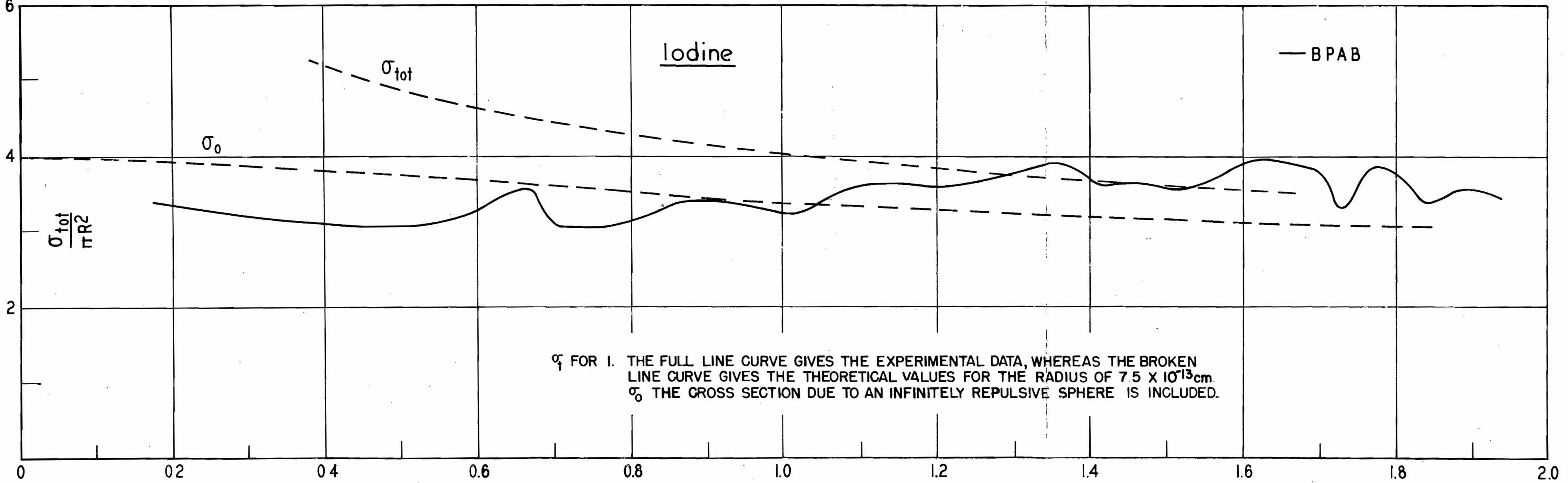


FIG. 10



σ_f FOR Sb. THE FULL LINE CURVE GIVES THE EXPERIMENTAL DATA, WHEREAS THE BROKEN LINE CURVE GIVES THE THEORETICAL VALUES FOR A RADIUS OF 8.5×10^{-13} cm. σ_0 THE CROSS SECTION DUE TO AN INFINITELY REPULSIVE SPHERE IS INCLUDED.

FIG. II
-78-



X = KR

FIG.12

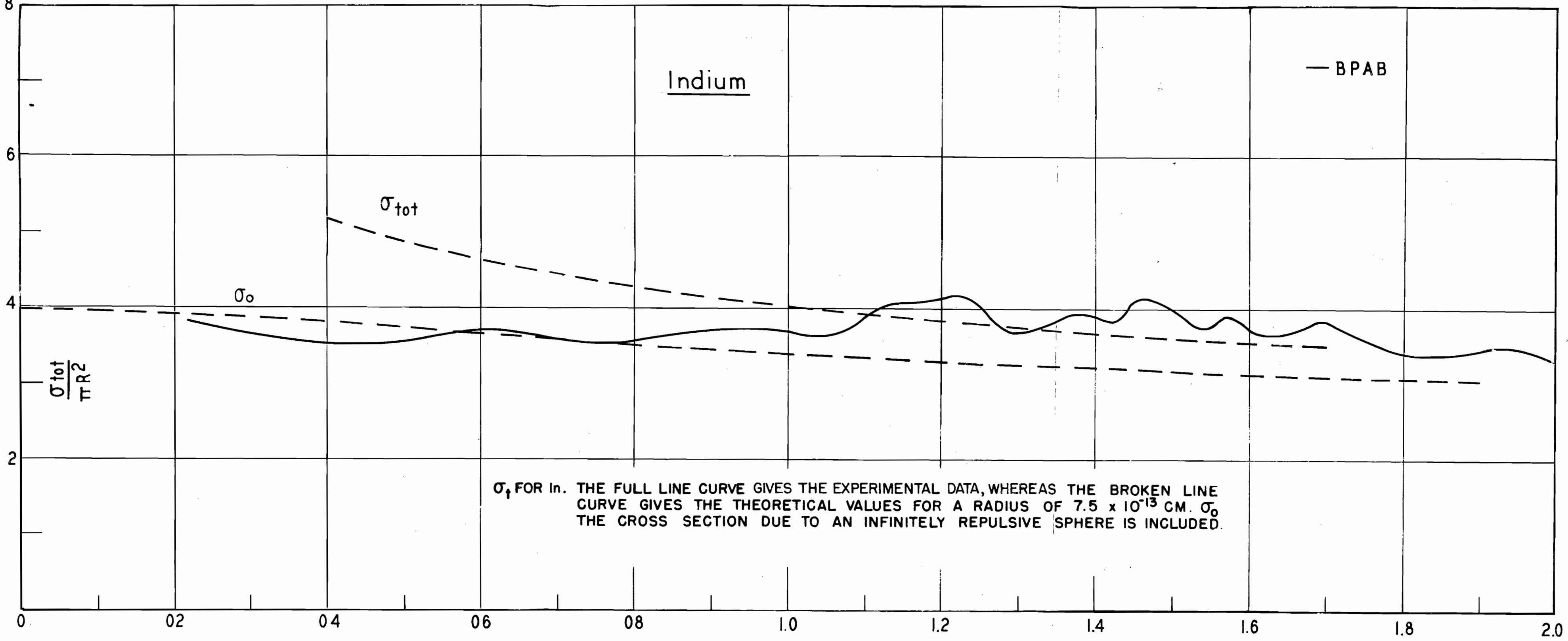


FIG. 13
-80-

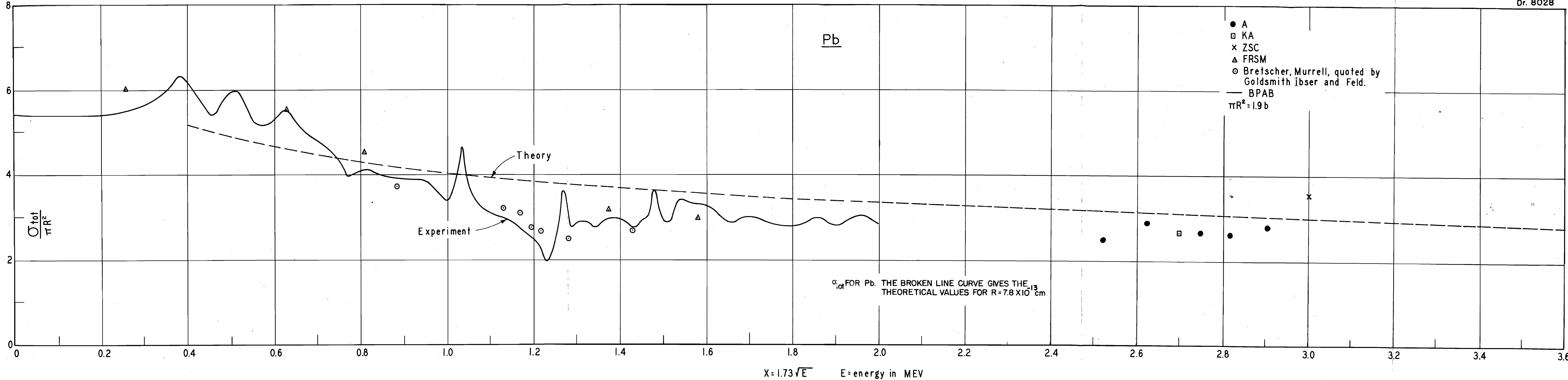


FIG. 14

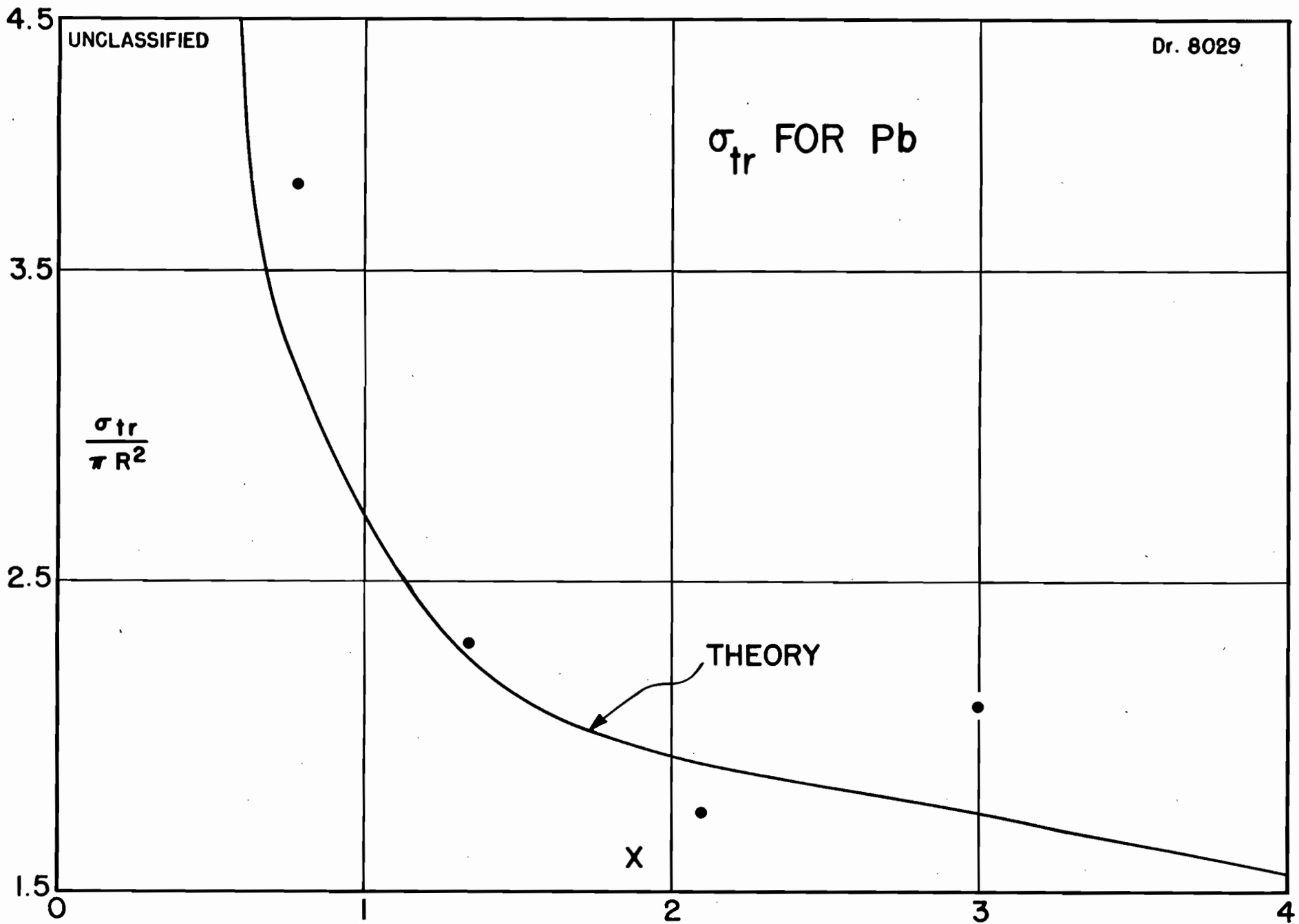


FIG. 15

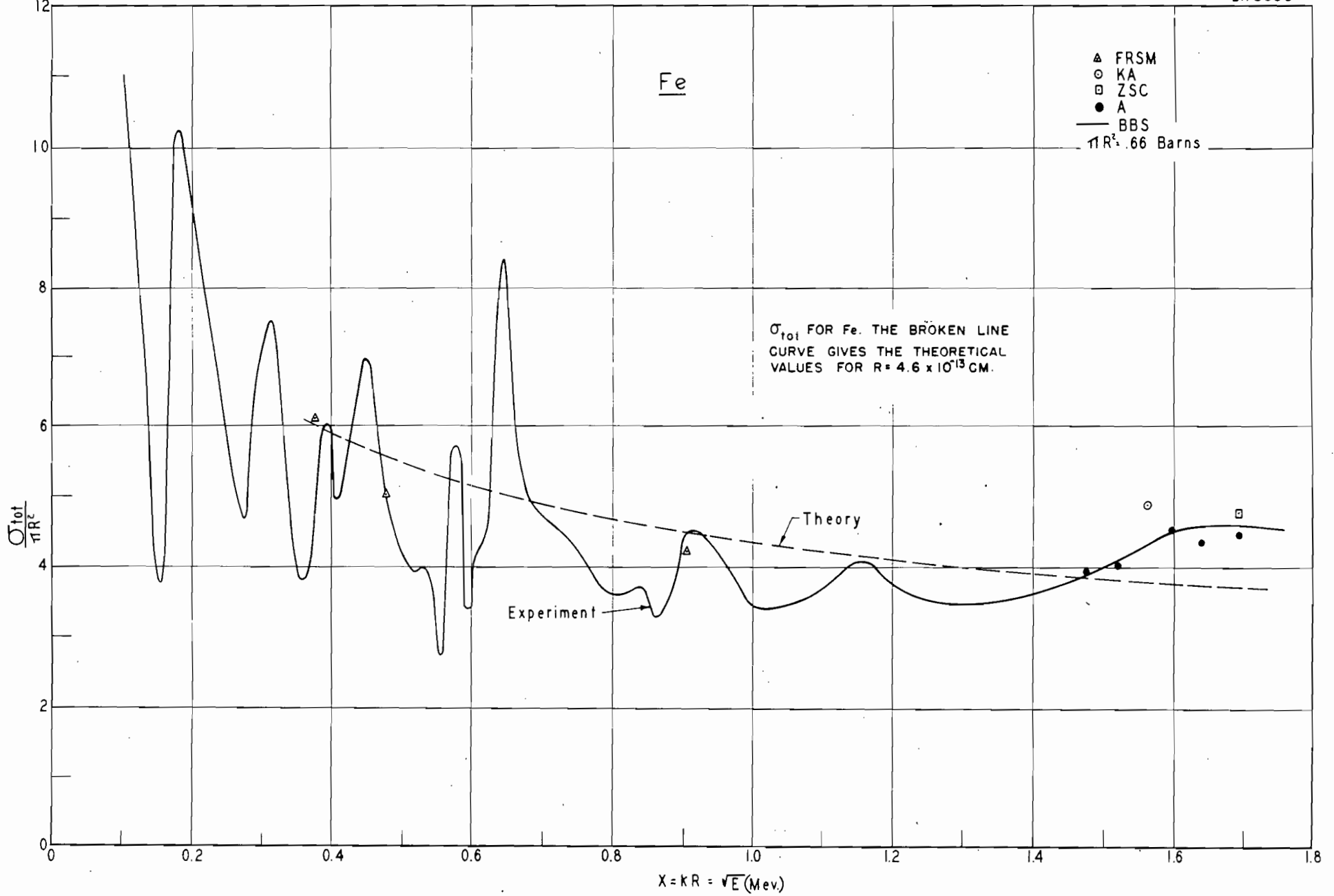


FIG. 16

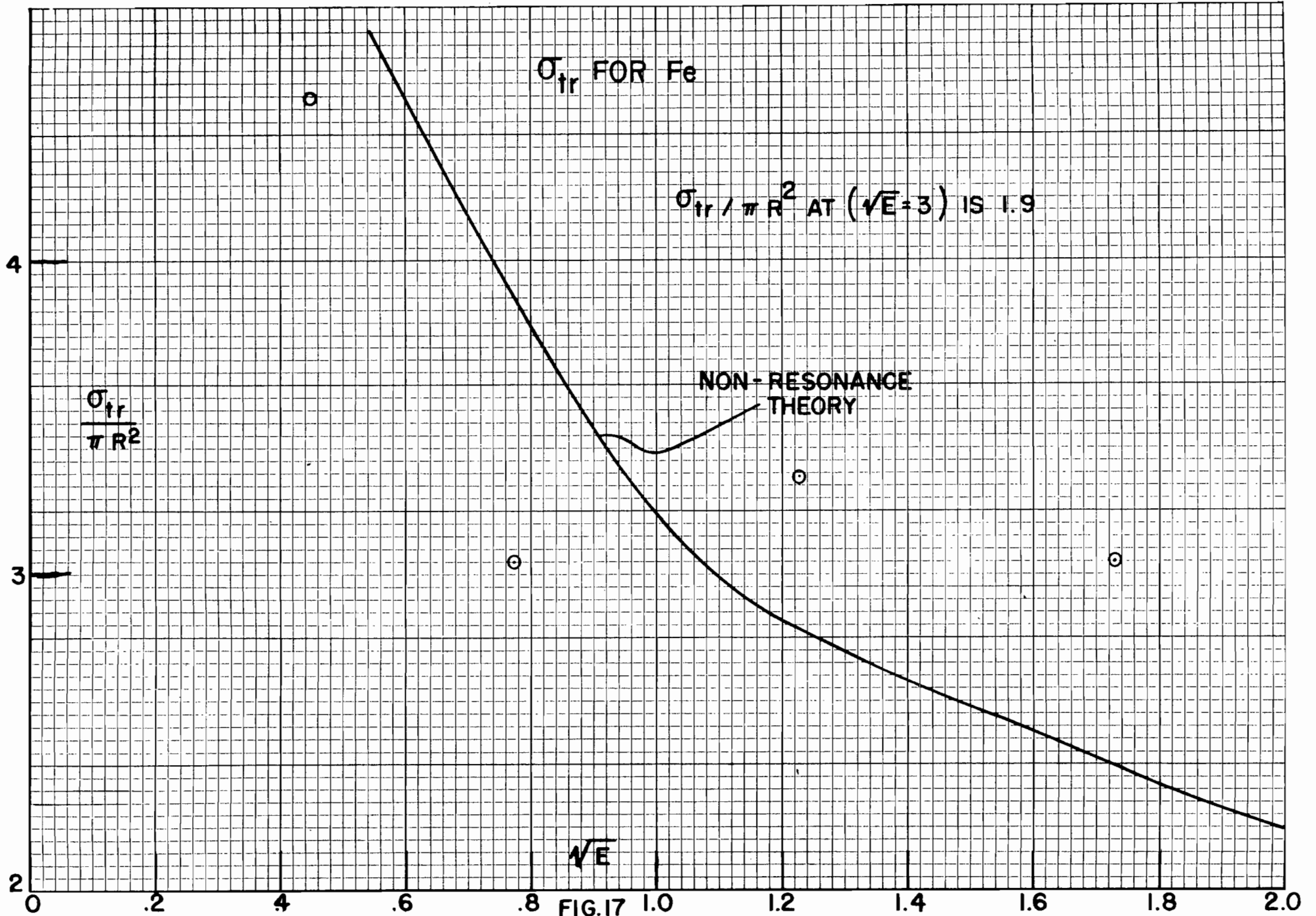


FIG.17
-84-

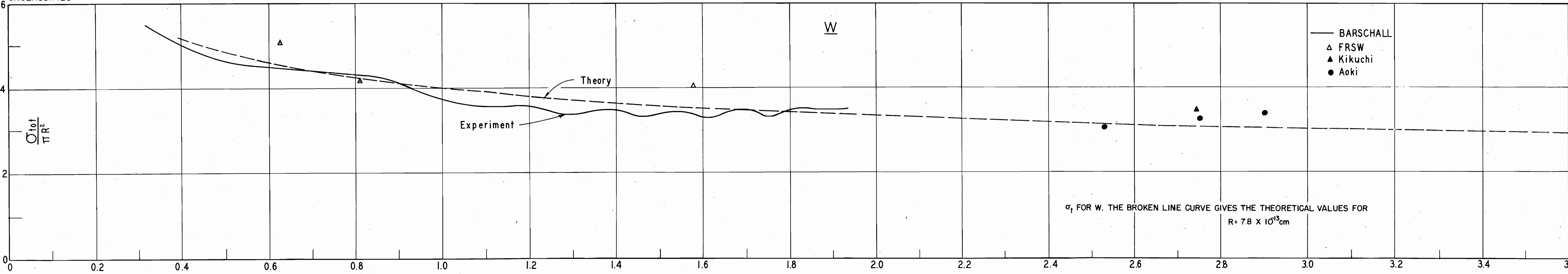


FIG. 18

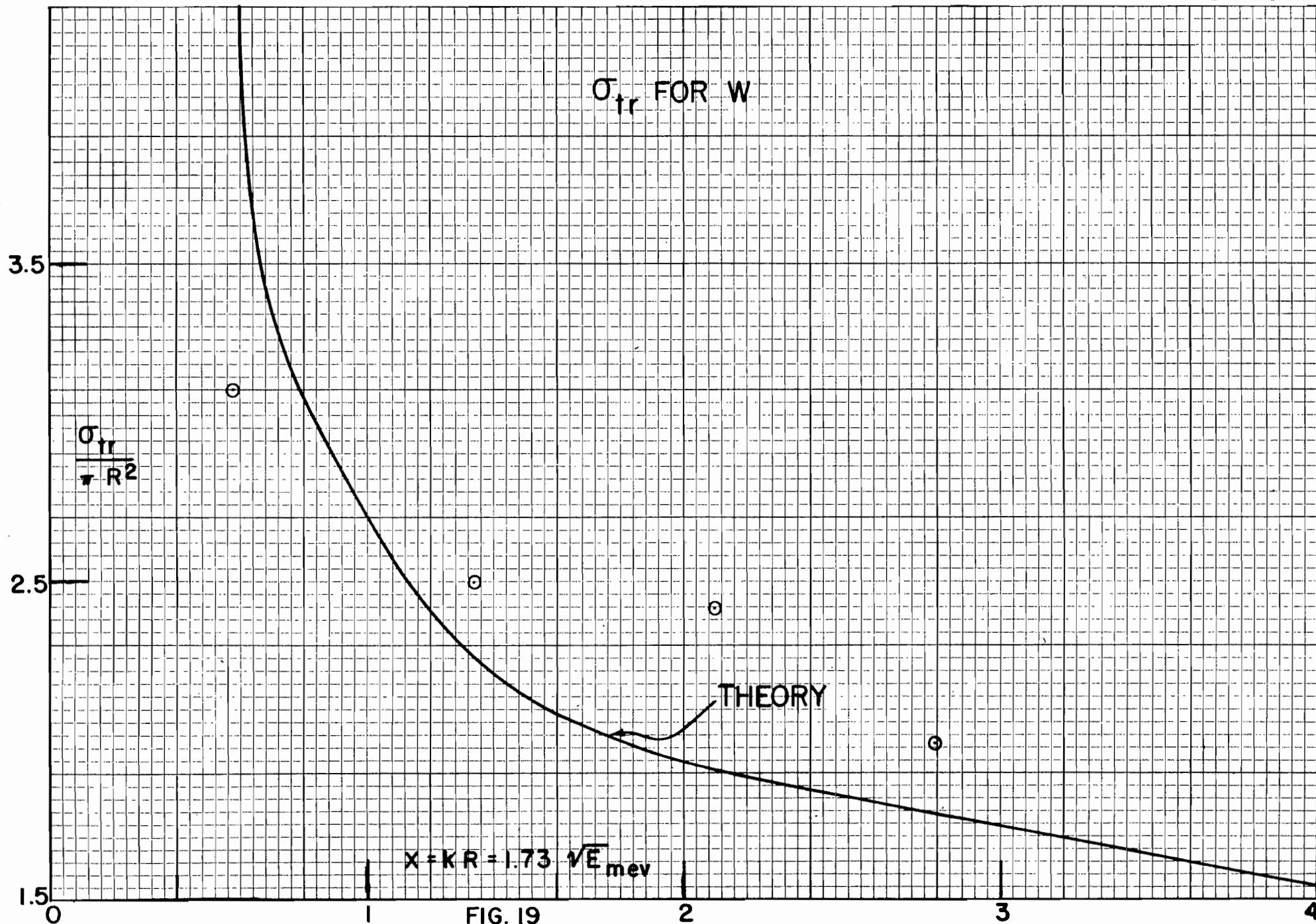
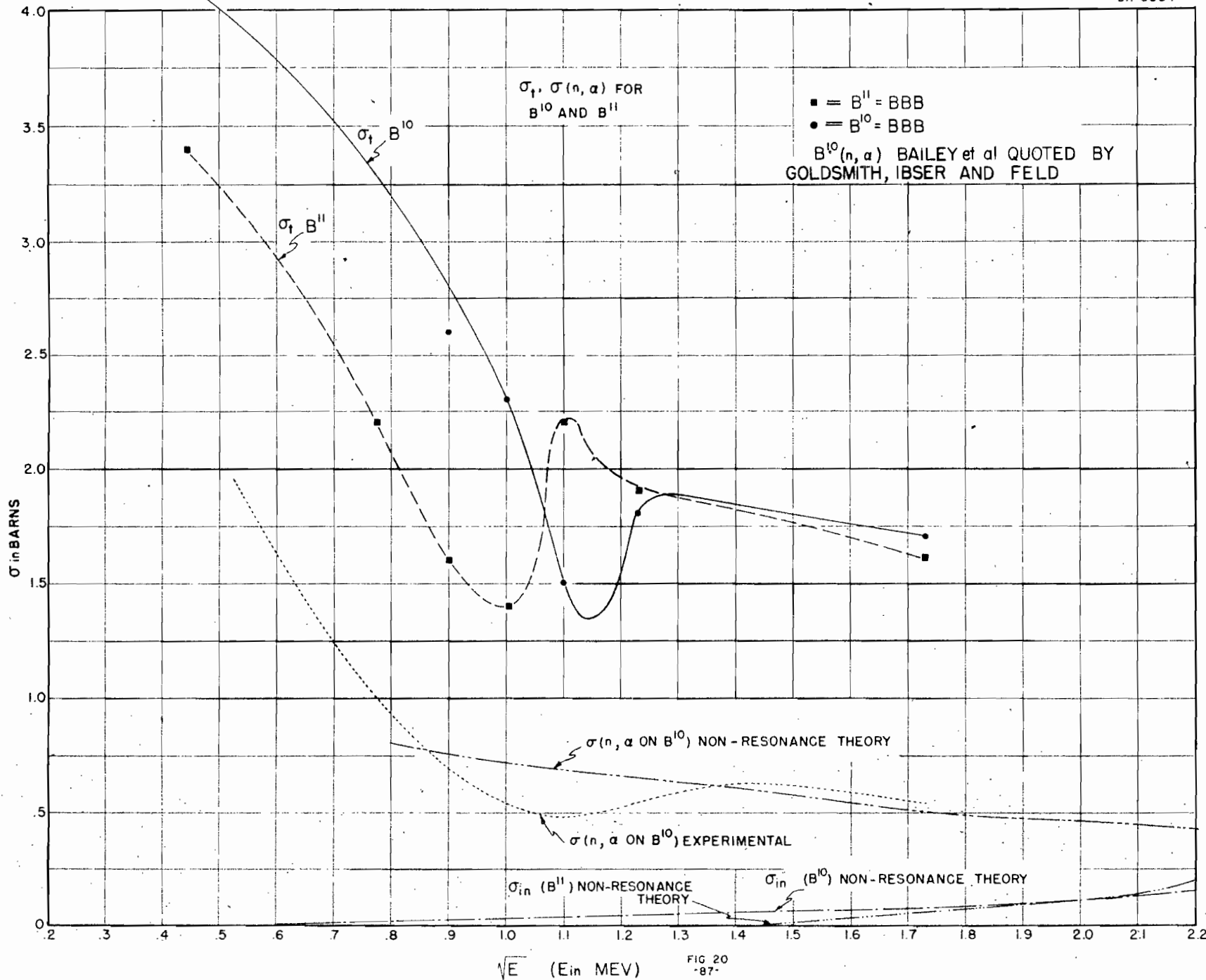


FIG. 19
-86-



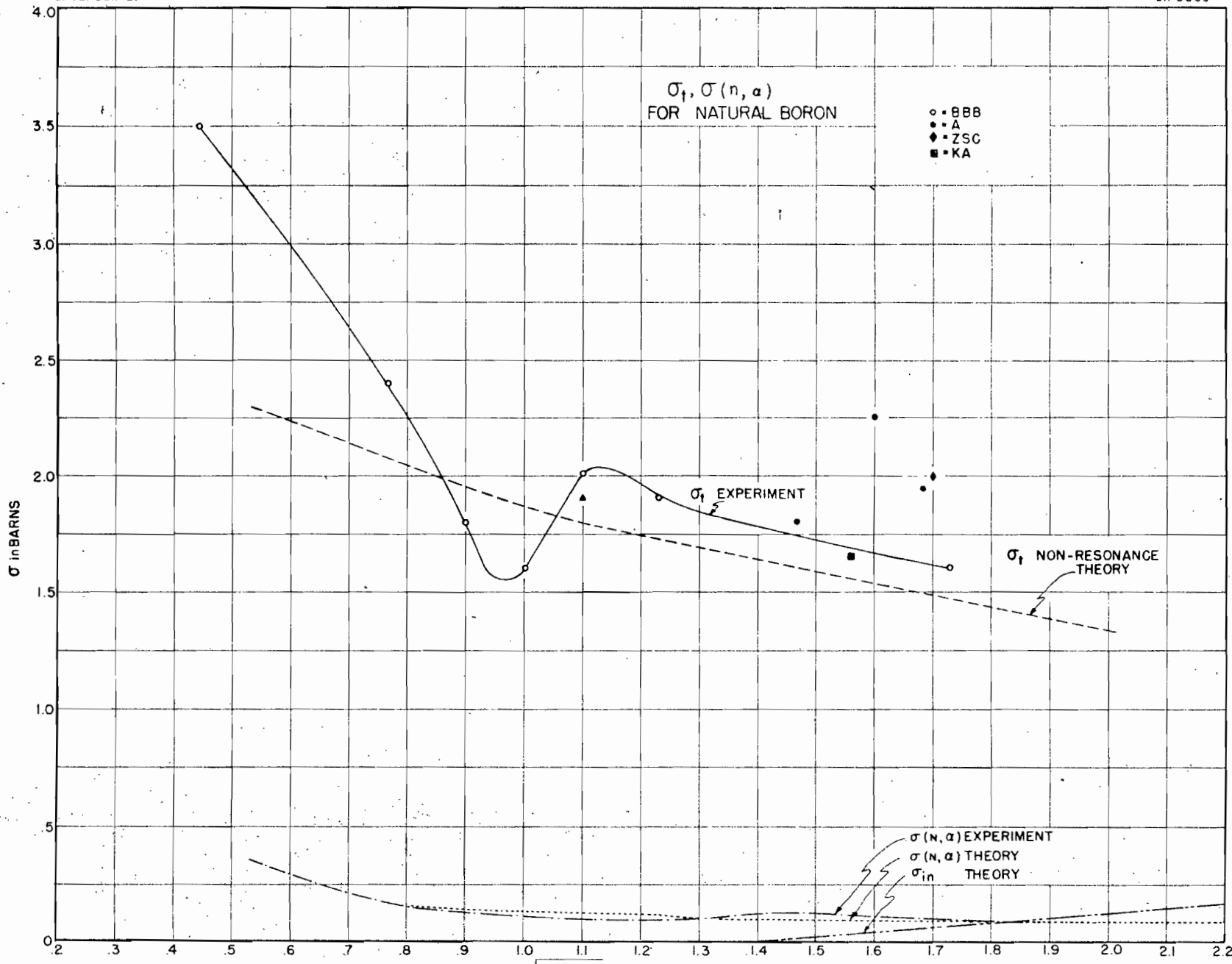


FIG 21
-88-

UNCLASSIFIED

Dr. 8064

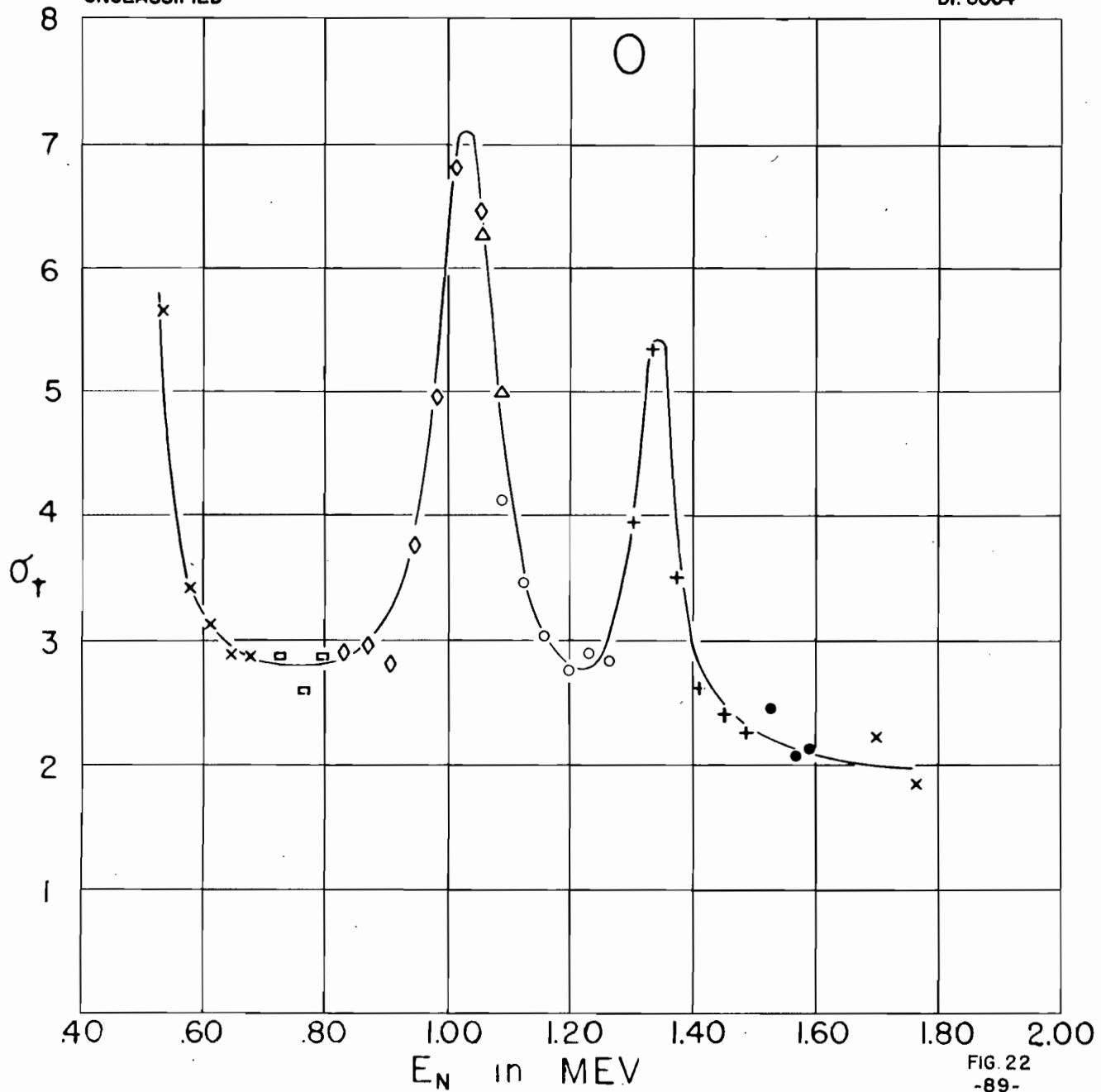
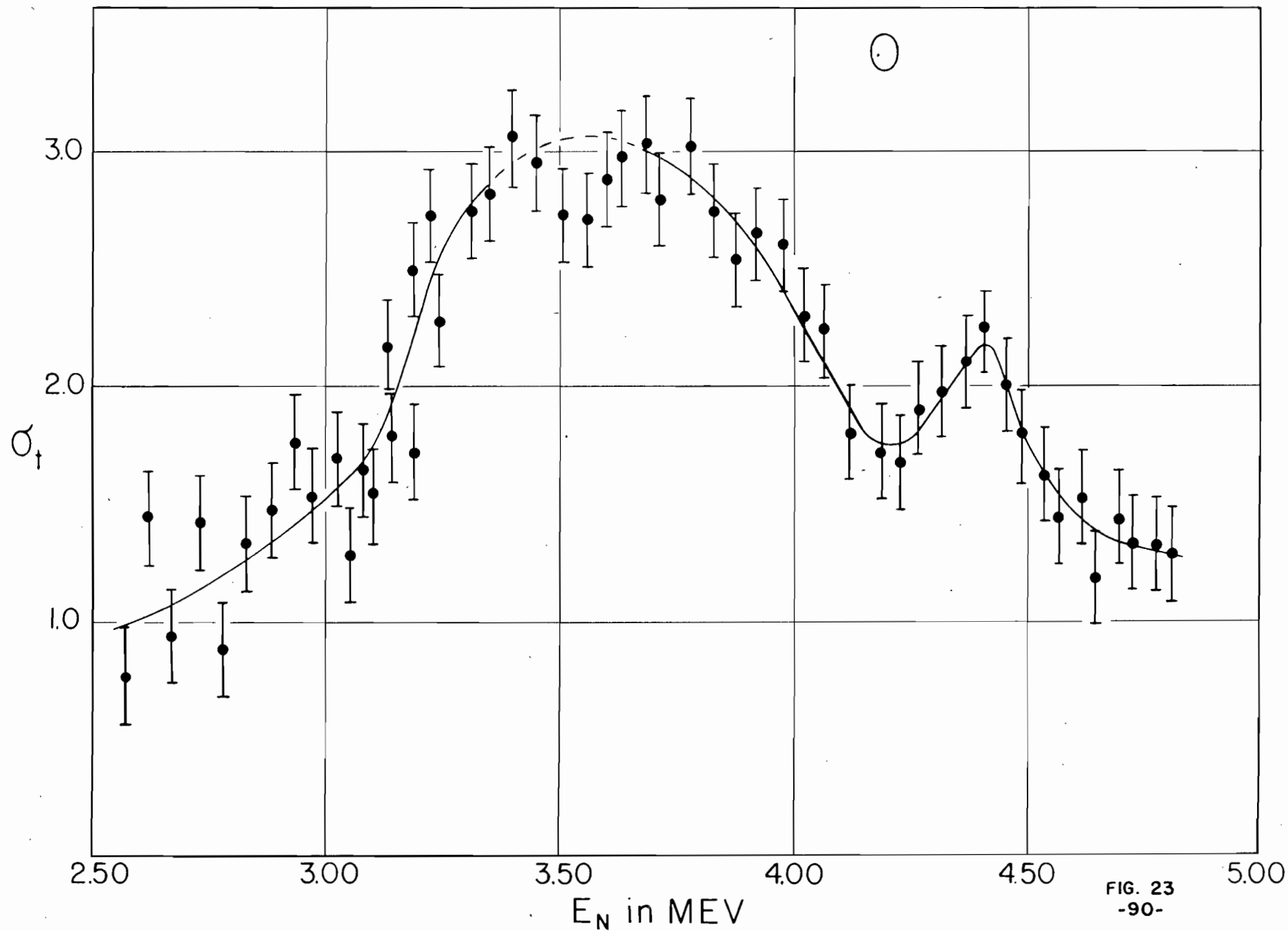


FIG. 22

FIG. 23
-90-

UNCLASSIFIED

Dr. 8066

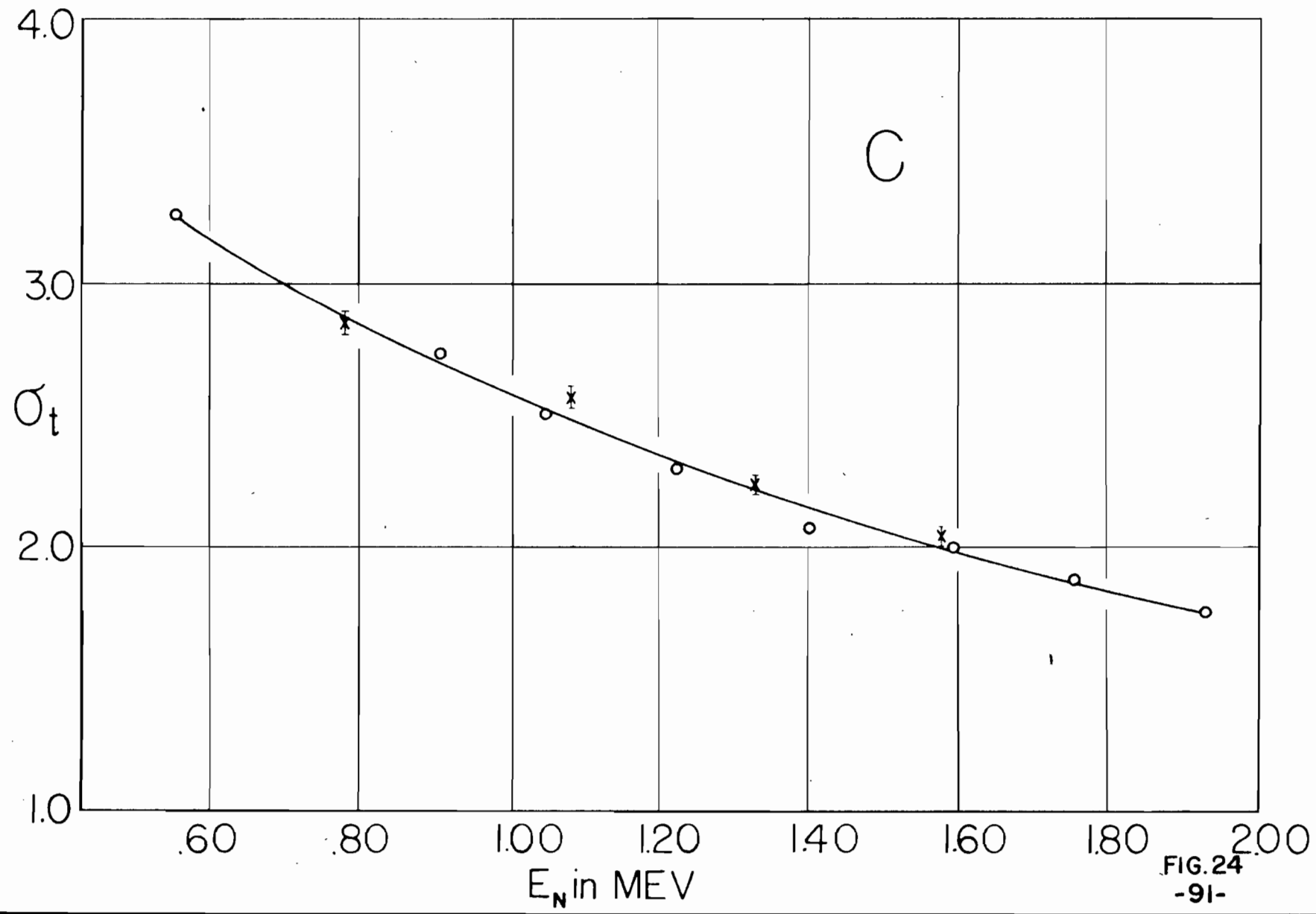


FIG. 24

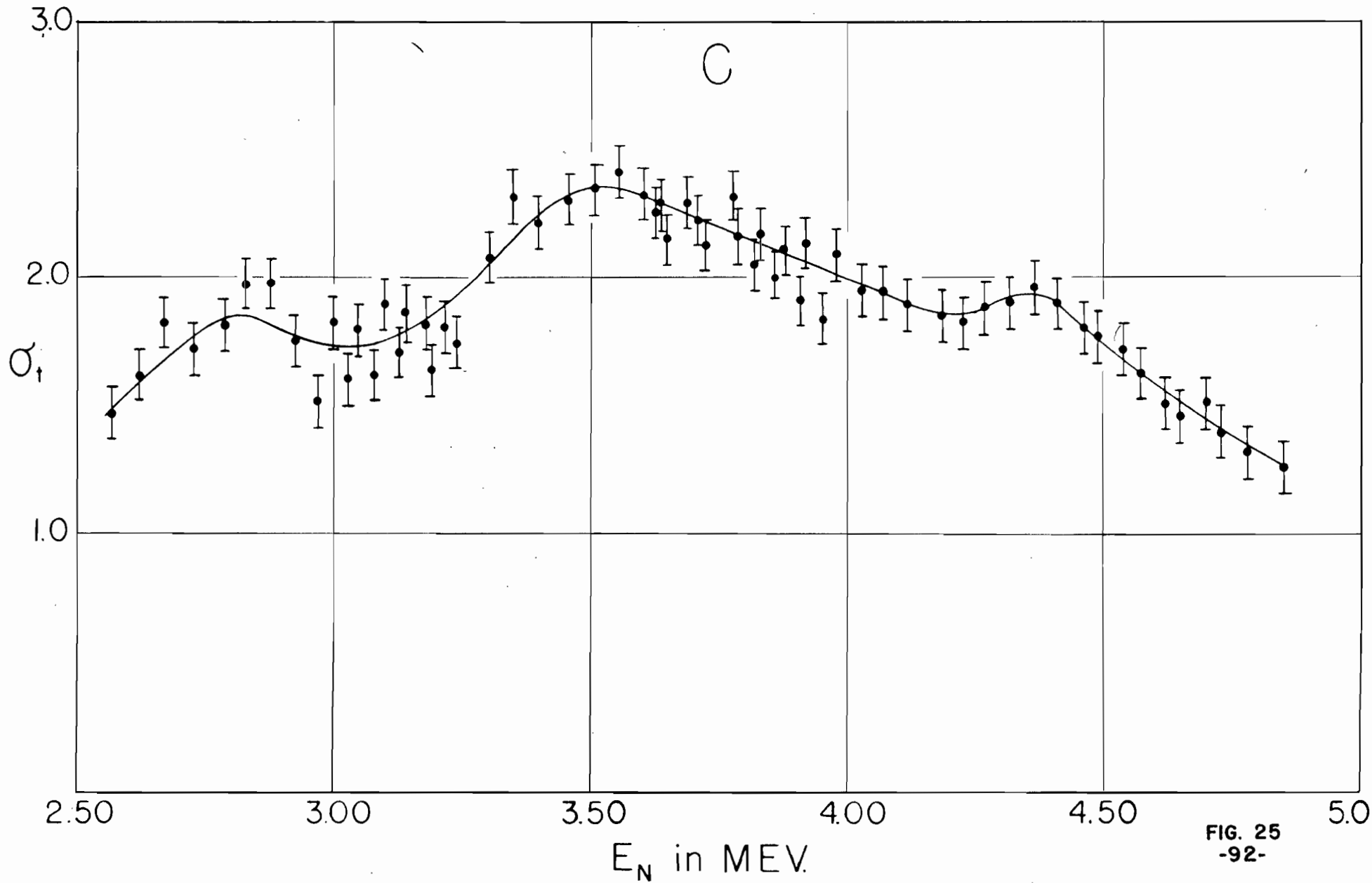


FIG. 25
-92-

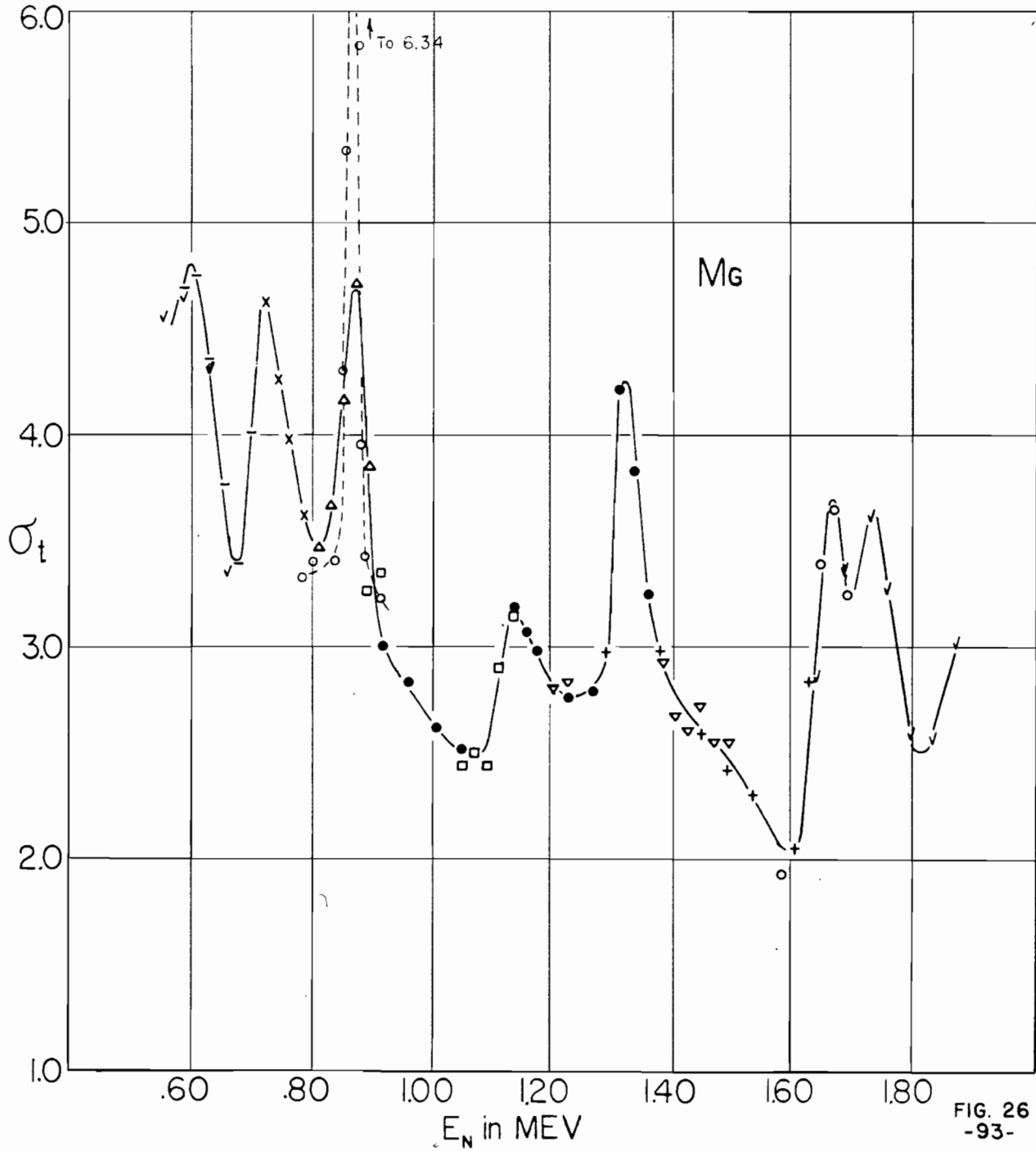
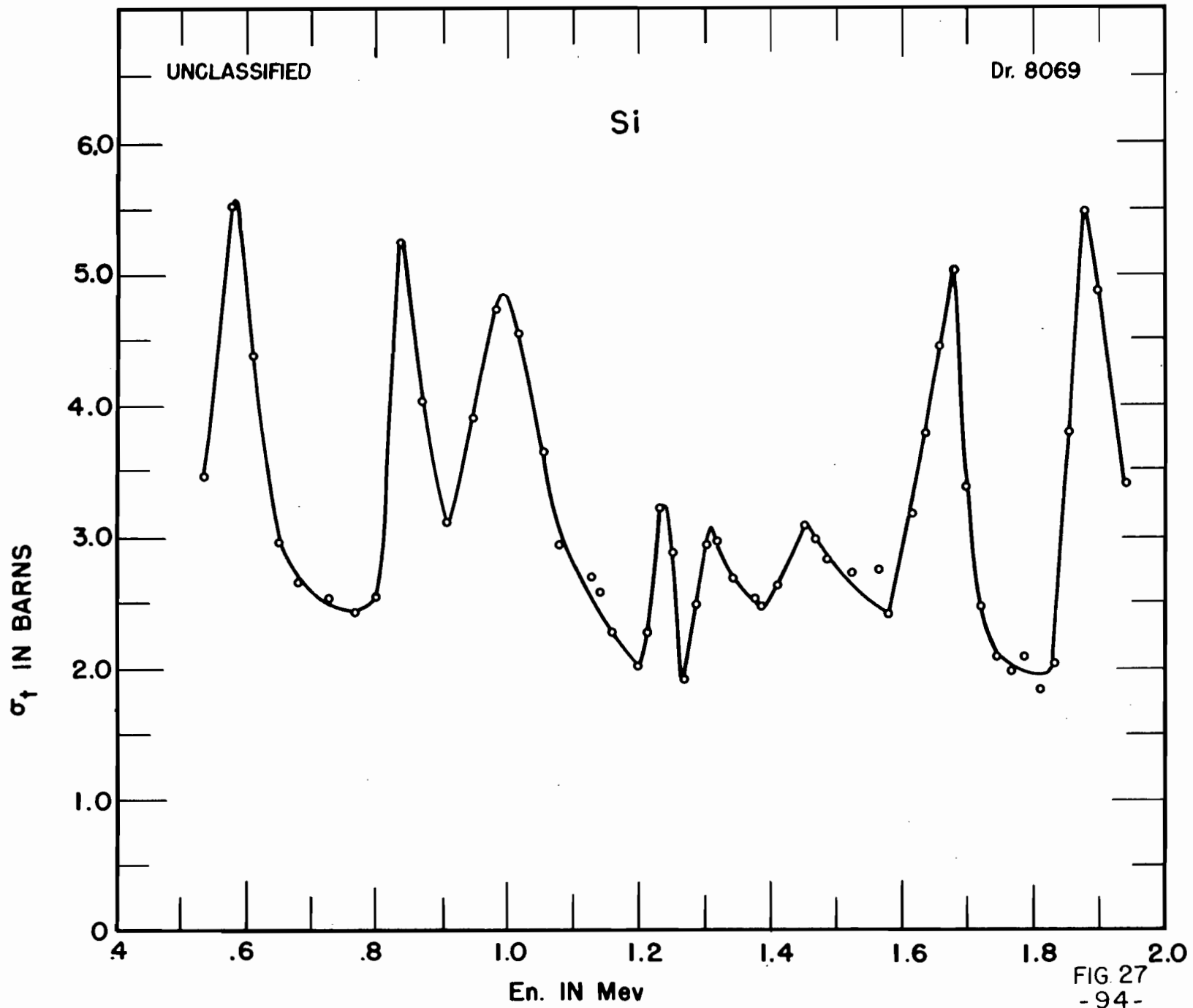


FIG. 26
-93-



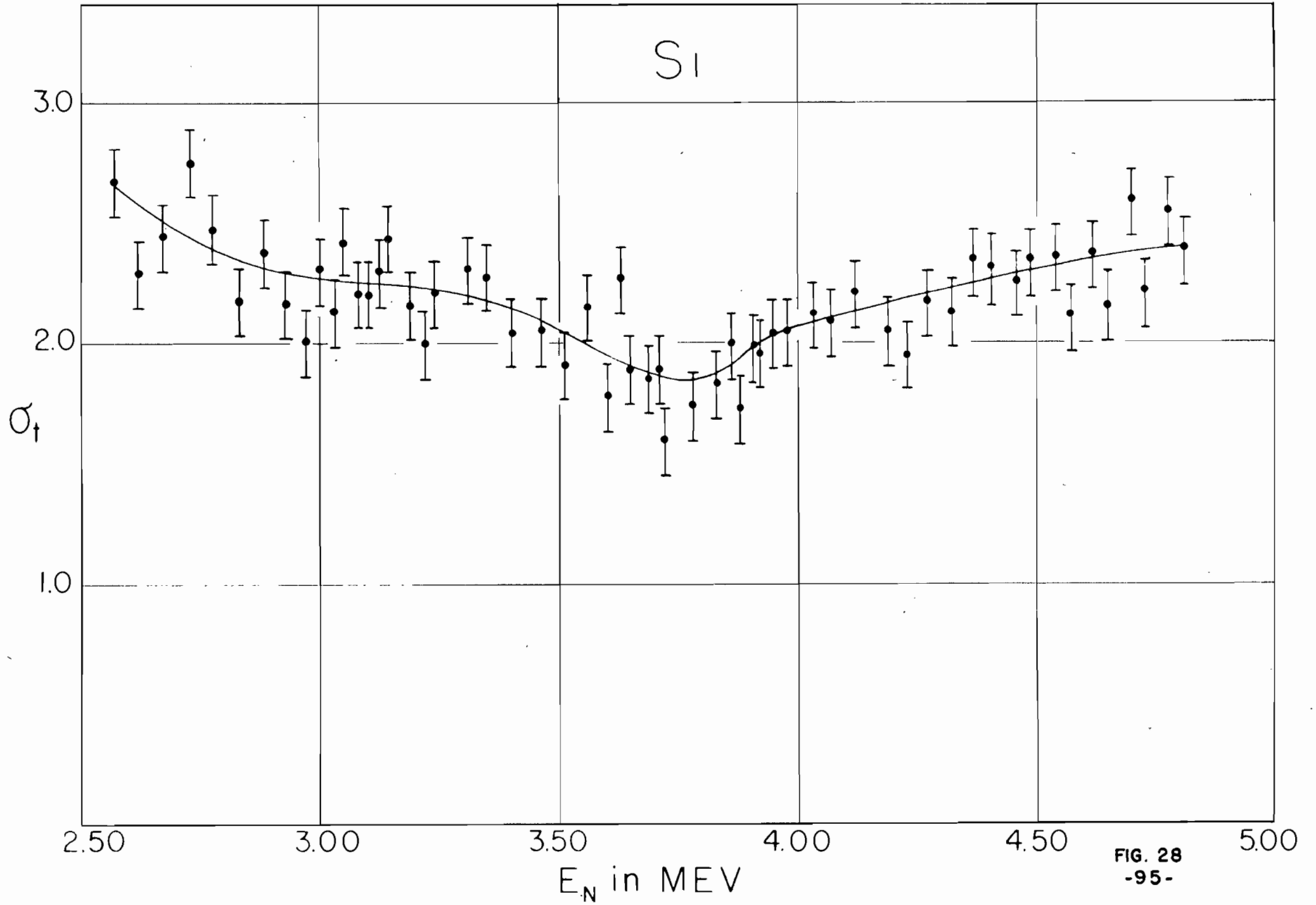


FIG. 28
-95-

UNCLASSIFIED

Dr. 8071

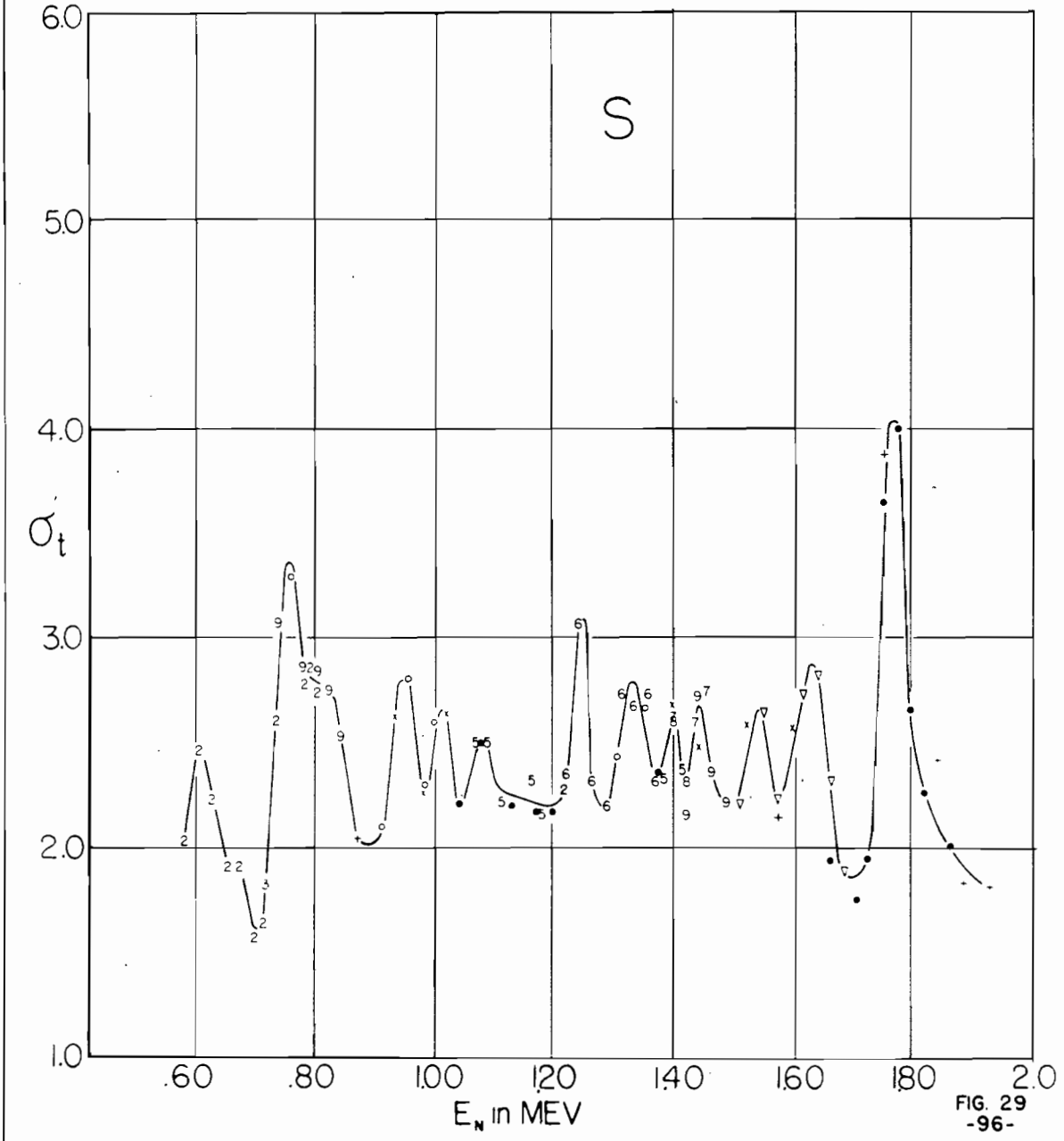


FIG. 29
-96-